JOURNAL OF GEOPHYSICAL RESEARCH, VOL. 97, NO. C3, PAGES 3543–3572, MARCH 15, 1992

Isopycnal and Diapycnal Circulation of the Upper Equatorial Atlantic Ocean in 1983–1984

YVES GOURIOU[1]

Institut Français de Recherche Scientifique pour le Développement en Coopération, Institut Français de Recherche pour l'Exploitation de la Mer, Plouzané, France

GILLES REVERDIN[2]

Lamont-Doherty Geological Observatory, Palisades, New York

Isopycnal circulation and diapycnal processes in the equatorial Atlantic Ocean are investigated using eight cruises from November 1982 to July 1984. An eastward decrease of the transport of the equatorial undercurrent is observed averaging 18.2 10^6 m^3 s^{-1} at 35°W to 10.2 10^6 m^3 s^{-1} at 4°W. There is also a meridional convergence at the undercurrent level and a larger meridional divergence in the surface layer of 15 10^6 m^3 s^{-1} between 35°W and 4°W. In the eastern equatorial Atlantic, the undercurrent core density as well as the salinity above the undercurrent experience a large seasonal cycle. During the season where the eastern Atlantic thermocline is closest to the surface and surface waters are coldest, the current peaks in denser waters and subsurface salinity maximum are weaker. An analysis of the salinity on isopycnal surfaces indicates that there is significant diapycnal mixing in the upper thermocline. In the eastern Atlantic, the upper thermocline vertical heat diffusivity coefficient scaled over 1° of latitude varies between 3 cm^2 s^{-1} during the upwelling season and nearly 0 early in the year. This seasonal mixing is an important element of undercurrent dynamics. The turbulent heat flux at the base of the surface layer averages 50 W m^{-2} between 1.5°N and 1.5°S. The surface layer heat budget implies an average oceanic gain of 60 W m^{-2} between 1.5°N and 1.5°S which could result from exchanges with the atmosphere. The heat flux and fresh water seasonal cycles needed to close the budgets are not realistic, however. The eastern equatorial Atlantic thermocline seasonal upwelling is associated with a large inflow into the surface layer. Over the two years, this flow averaging 11–12 × 10^6 m^3 s^{-1} originates from the upper thermocline, and diapycnal transports near the core of the undercurrent or below are found to be small. Below the core of the undercurrent, we also find that mixing is not intense: for instance, at $\sigma_\theta = 26.5$, in the upper part of the thermostad, vertical heat diffusivity is only 0.6 cm^2 s^{-1} (assuming that mixing takes place over 1° of latitude). The uncertainties on these budgets are however large, and assumptions on the dynamics that were used could not be checked.

1. INTRODUCTION

The sea surface temperature in the equatorial Atlantic exhibits a pronounced seasonal cycle, particularly in the eastern equatorial Atlantic [*Merle et al.*, 1979; *Picaut*, 1983]. A cold water tongue appears there from May to September (Figure 1*a*), initially centered at the equator or slightly to the south in the Gulf of Guinea [*Voituriez*, 1983], coincident with an uplift of the thermocline [*Merle*, 1980]. This area is heated by the atmosphere [*Hastenrath and Lamb*, 1978], and requires therefore, a subsurface source for cooling. A subsurface water influx is also indicated by the presence of dissolved inorganic nutrients in the surface waters. Total dissolved inorganic carbon and dissolved carbon dioxide are also larger near the equator than in subtropical waters, which induce a degasing of carbon dioxide toward the atmosphere [*Smethie et al.*, 1985; *Andrié et al.*, 1986; *Garçon et al.*, 1989]. There is also an equatorial minimum in surface anthropogenic tracers, as shown for tritium and radiocarbon in *Broecker et al.* [1978] and *Broecker and Peng* [1982].

Two mechanisms which explain this cold water tongue have been documented [*Voituriez*, 1981]. One is the upwelling of subsurface layers when the equatorial thermocline is uplifted as a result of the large-scale dynamics. The second is that vertical mixing between the surface waters and the Equatorial Undercurrent varies seasonally, which would modulate the entrainment into the surface layer.

The two processes are indistinguishable for the upper layer. On the other hand, the presence or absence of this vertical mixing is important in subsurface layers. Mixing would induce a subsurface water-mass transformation. How deep this happens does influence whether the seasonally surfacing waters originate from fairly shallow horizons or are part to the much deeper upwelling envisioned for the equatorial band (for instance, in *Broecker et al.* [1978]). Dynamics in the thermocline could also be strongly influenced by this mixing. In the Pacific, large-scale observations presented in *Dillon et al.* [1989] and *Wilson and Leetmaa* [1988] suggest that small-scale mixing has major effects on the upper thermocline eastward flow. This was also discussed for the Atlantic Equatorial Undercurrent (EUC) based on a few microstructure profiles [*Crawford and Osborn*, 1979*b*] (major currents are depicted on Figure 2*a*). Model studies presented in *Wacongne* [1989] suggest a large effect of mixing in the central equatorial Atlantic thermocline.

[1]Temporarily at Woods Hole Oceanographic Institution, Woods Hole, Massachusetts.
[2]Also at Laboratoire d'Océanographie Dynamique et de Climatologie, Université Paris VI, Paris, France.

Paper number 91JC02935.
0148-0227/92/91JC-02935$05.00

In this paper, we will attempt to clarify these questions from upper ocean budgets based on a set of seasonal cruises in the Atlantic Ocean in 1982–1984. We will review the evidence for mixing before describing approaches used to infer mixing and vertical transports.

Microstructure data show an intense mixing zone in the upper equatorial thermocline, both in the Atlantic and in similar situations in the Pacific Ocean [*Crawford and Osborn*, 1979*a*; *Osborn*, 1980]. *Osborn* [1980] suggested that the mixing was induced by the shear between the surface current and the Equatorial Undercurrent. However, the latitudinal extension of the upper thermocline strong mixing is still debated from a 10-day set of microstructure profiles in the equatorial Pacific Ocean: *Moum et al.* [1989] argue that the vertically integrated turbulence does not peak above the undercurrent, but *Peters et al.* [1989] show that the subsurface turbulence maximum is at the latitude of the EUC core.

Niiler and Stevenson [1982] and *Reverdin* [1984] estimate an average turbulent heat flux across the 25°C isotherm from the net air–sea heat flux in the warm water sphere. For a mixing within 1.5° of the equator, this corresponds to 100–150 W/m^2 turbulent heat flux. However, error bounds are large so that this is not significantly nonzero. The subsurface hydrography also contains evidence for mixing. It has long been known that maximum salinity associated with the undercurrent and tracing water of southern origin [*Metcalf and Stalcup*, 1967] eroded eastward [*Neumann et al.*, 1975], and that this erosion varied seasonally [*Neumann*, 1972]. Part of this relates to the upwelling of the upper thermocline saltier water into the central Atlantic surface layer. However, the effect is still present when the analysis is carried on isothermal or isopycnal surfaces which do not reach the sea surface. Based on these ideas, *Katz et al.* [1979] quantified the turbulent mixing from a set of nearly simultaneous cruises in June 1974, yielding a vertical heat eddy

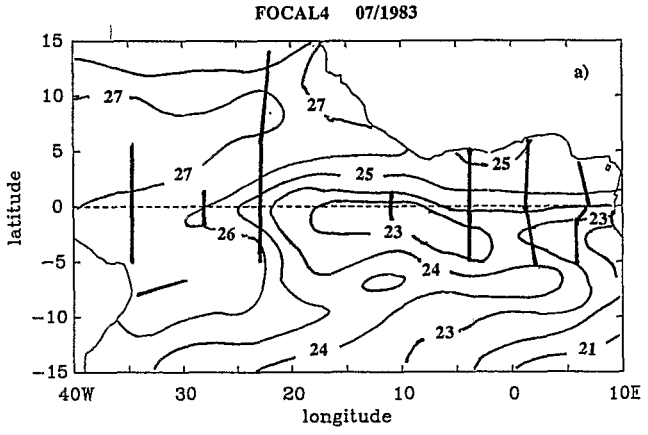

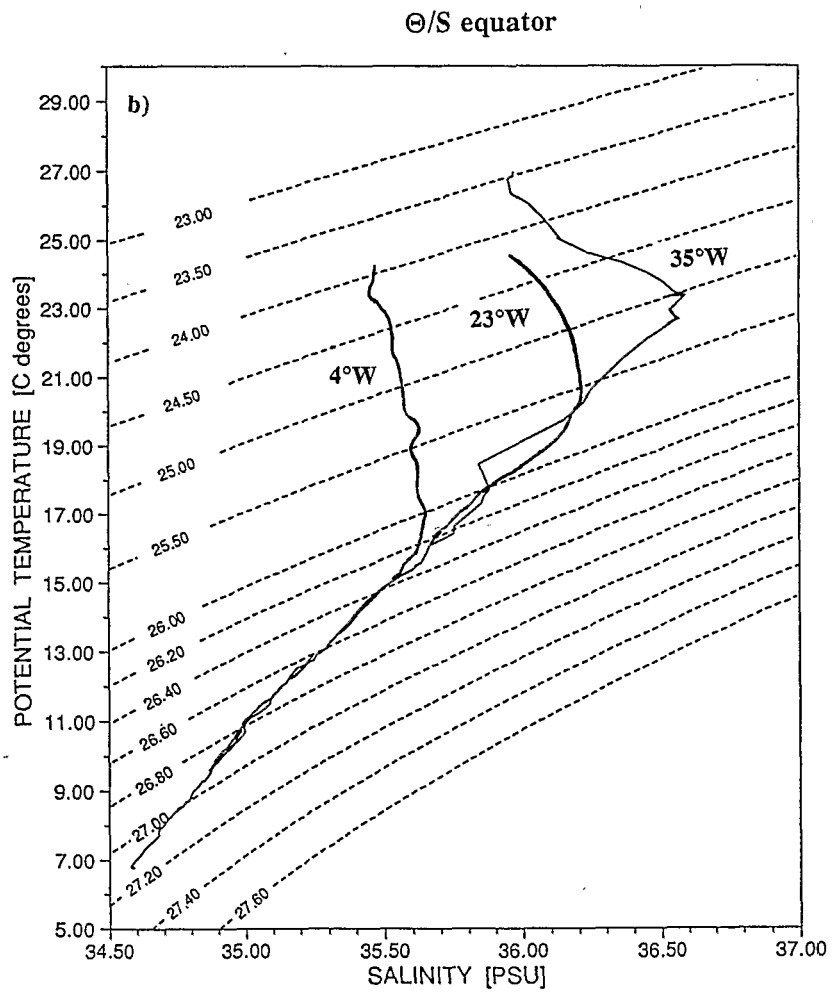

Fig. 1. July 1983 FOCAL 4 cruise. (*a*) Positions of stations and sea surface temperature analyzed for July 1983 combining hydrographic stations with other surface data. (*b*) θ–S relationships for three stations corresponding to the EUC core. The easternmost profile along 4°W is also typical of profiles in the central and eastern Atlantic a few degrees north of the equator during 1982–1984.

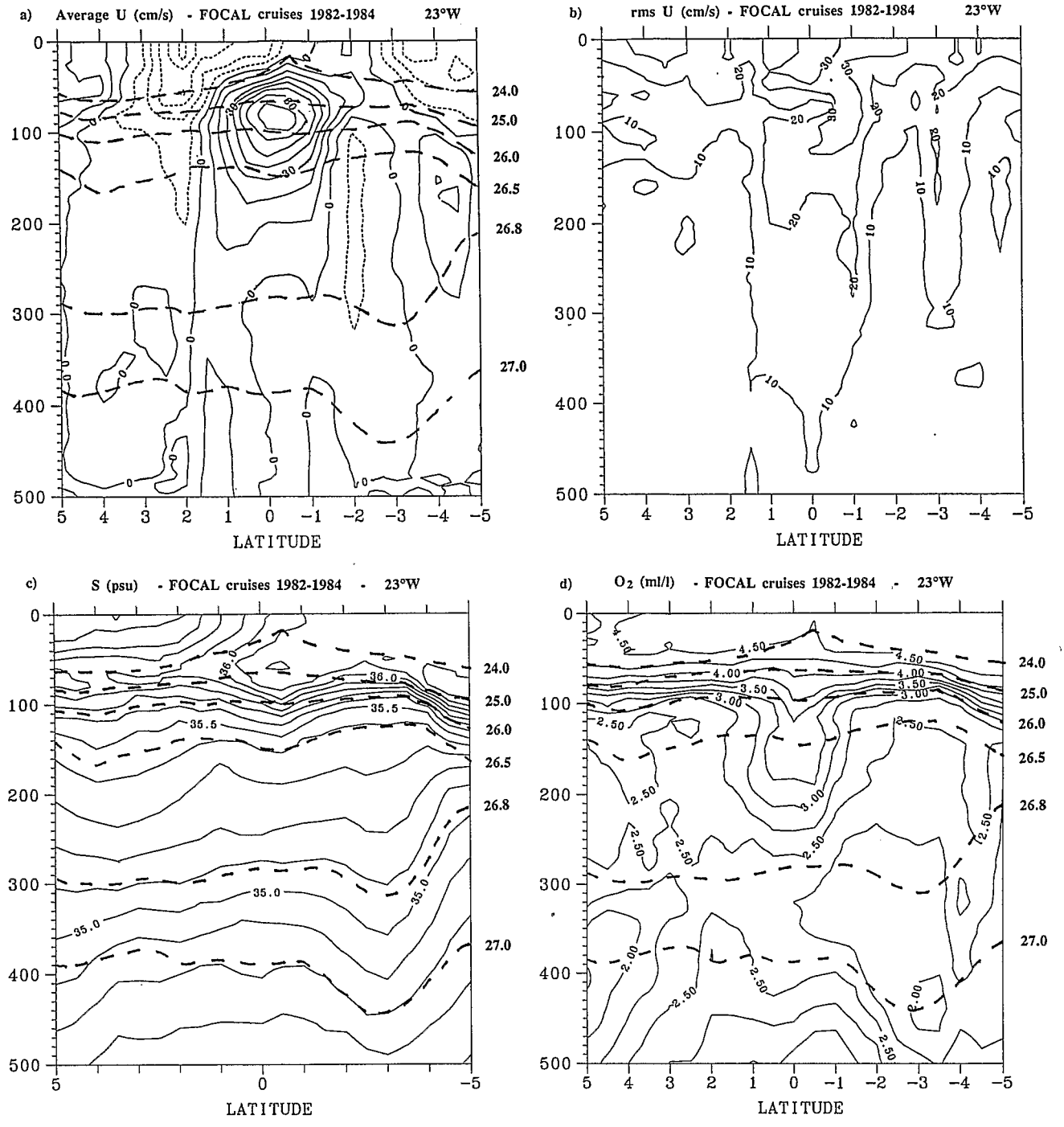

Fig. 2. Composite 23°W section from the seven FOCAL cruises along 23°W (most sections have a 0.5° spacing, and for the rare exceptions, linear interpolation to the 0.5° grid has been done). A few selected isopycnals are plotted with dashed line. (*a*) The average zonal current section, currents are not measured above 20 m. (*b*) The unbiased estimate of the current rms standard deviation. (*c*) Average salinity, (*d*) Average dissolved oxygen (mL/L).

coefficient of 1.5 cm^2/s. That data set was insufficient to take into account time variability.

Vertical mixing induces a mean flow across isopycnal surfaces: the diapycnal circulation discussed in *McDougall* [1984]. In the upper equatorial Atlantic thermocline, horizontal mixing is expected to have secondary importance [*Weisberg and Weingartner*, 1988], so that the diapycnal velocity induced by mixing of different waters with the same density is likely to be small. Therefore, potential temperature $\{\theta\}$ and salinity evolution on isopycnal surfaces is controlled by two diapycnal processes: heating by penetrating solar radiation ($\dot{Q}_z$) and small-scale vertical mixing associated with a diapycnal velocity ω. Assume that the small-scale eddy fluxes $\{\omega'\theta', \omega'S'\}$ are related to local gradients as $\{\overline{\omega'\theta'}, \overline{\omega'S'}\} = -\{K_\theta\, d\theta/dz, K_S\, dS/dz\}$, where K_θ, K_S are the vertical diffusivity coefficient. If double diffusive effects are small, an equation for the diapycnal velocity ω is obtained by combining the salinity and the temperature equations (Appendix A):

$$\omega = K_z + \frac{\rho_\theta \theta_{zz} + \rho_S S_{zz}}{\rho_z} K + \rho_\theta \frac{\dot{Q}_z}{\rho c_p \rho_z} \qquad (1)$$

where ρ is the potential density referred to the average depth considered, $\{\rho_\theta, \rho_S\} = \{\partial\rho/\partial\theta_{|S,P}; \partial\rho/\partial S_{|\theta,P}\}$ are the expansion coefficients of potential density with respect to potential temperature and salinity, c_p is the heat capacity, and K is the diffusivity coefficient. Therefore, diagnostically, the knowledge of the diffusion profiles can be used to deduce profiles of vertical velocity (and vice versa).

However, it is difficult to use (1) to infer the diapycnal circulation related to mixing. More direct approaches have also been used. In the equatorial Pacific thermocline, ω has been deduced as a residual using the continuity equation, either from large-scale hydrographic and current surveys [*Bryden and Brady*, 1985] or current meter arrays [*Halpern et al.*, 1989; *Brady and Bryden*, 1987; *Bryden and Brady*, 1989]. In the Atlantic, a moored array near 28°W has been used to derive vertical circulation [*Weingartner and Weisberg*, 1991]. These methods provide coherent estimations of an average value, but their uncertainty is too large to provide reliable seasonal variability.

Our first approach will be to estimate average circulation (u, v) along isopycnals or other surfaces (depth $h(\sigma, x, y)$). The continuity equation is integrated vertically to estimate the average diapycnal velocities (ω) and the "upwelling" (mass flux) into the surface layer as:

$$\omega = -\int \left\{ \left(\frac{dh}{d\sigma}u\right)_x + \left(\frac{dh}{d\sigma}v\right)_y \right\} d\sigma$$

where stationarity is assumed. To estimate the turbulent fluxes, equation (1) could be used. However, because the term in front of K is very uncertain, this is not a recommended approach. Average turbulent heat and salinity fluxes can also be estimated from the simplified average heat and salinity budget:

$$\left(\frac{dh}{d\sigma}Au\right)_x + \left(\frac{dh}{d\sigma}Av\right)_y + \frac{d(A\omega)}{d\sigma} = -\frac{d(\overline{A'\omega'})}{d\sigma} + \frac{dQ}{d\sigma} \quad (2)$$

where A is one of the variables and $dQ/d\sigma$ possible sources or sinks. *Bryden and Brady* [1985] have similarly analyzed heat fluxes required by their diagnostic circulation of the equatorial Pacific with encouraging results. If circulation was well known, time evolution could also be included in this set of equations.

The second approach analyzes the salinity budget on isopycnal surfaces as in *McDougall* [1984]. Vertical velocity is replaced by (1) in the equation of conservation of salinity on an isopycnal surface, which can be rewritten as:

$$\left(\frac{\partial S}{\partial t}\right)_{\sigma_\theta} + U\nabla_{\sigma_\theta} S = -DK - \rho_\theta \frac{S_z \dot{Q}_z}{\rho c_p \rho_z} \quad (3)$$

where

$$D = \frac{\rho_\theta}{\rho_z} S_z^2 \left(\frac{\theta_z}{S_z}\right)_z$$

σ_θ denotes the isopycnal surface (we make the further justifiable approximation to refer the potential density to the sea surface). Advection along isopycnal surfaces will be evaluated, and from this budget, K and turbulent heat and salinity fluxes will be estimated. This equation also illustrates that with a Fickian approximation for the turbulent fluxes, an evolution of salinity along isopycnal surfaces can happen only when there is a curvature in the θ–S relationship. Evolution of S for a $D = 0$ would imply that one of the approximations does not hold. However, there is a noticeable curvature above $\sigma_\theta = 25.8$ (Figure 1*b*) in the western equatorial Atlantic waters off Brazil which flow into the EUC [*Metcalf and Stalcup*, 1967]. Therefore there is hope that this approach applied seasonally on the EUC salt tongue can provide information on the diapycnal fluxes seasonal variability.

Both approaches will be used with the 1982–1984 set of eight large-scale surveys. First, the data will be presented and data interpolations to estimate a seasonal cycle discussed. The relevance of this seasonal cycle for the real ocean is discussed in Appendixes B and C. In section 3, we will discuss zonal and meridional circulation. A section is devoted to seasonal budgets, where the salinity budget (3) is integrated between the observed sections along 35°W, 23°W and 4°W to estimate mixing. Finally, the average diapycnal transports are estimated from the integration of the continuity, heat and salt equations. Section 6 covers the comparison of the different approaches used and the results of other studies.

2. DATA

The R.V. *Capricorne* conducted research cruises every 3 months between October 1982 and July 1984 (to be referred as the FOCAL cruises). The stations considered in this paper are primarily along 35°W, 23°W and 4°W between 5°N and 5°S which samples the main domain of the cold tongue (Figure 1*a*) [*Hénin et al.*, 1987; *Hisard and Hénin*, 1987]. We also include additional stations further east for the averaged budget [*Hénin et al.*, 1987; *Piton and Wacongne*, 1985].

At each station, vertical profiles of pressure, temperature, conductivity and dissolved oxygen down to 500 m are collected by a Neil-Brown Mark III CTD. The current profile is obtained with a profiler equipped with an Aanderaa RCM 4 current meter under a surface buoy deployed from the vessel. Near the equator the stations are usually located on a regular grid every 0.5° of latitude, which constitutes our analysis grid. However, during the October 1982 FOCAL 1 and the January–February 1983 FOCAL 2 cruises, some stations within 5° of the equator were separated in latitude by 0.75°. In instances where no station was collected at a grid point, a profile is created by linear interpolation between the closest profiles. No current was measured during FOCAL 2 (January–February 1983) along 35°W and 23°W, and the 35°W section was not sampled during FOCAL 5 (October 1983). *Hisard and Hénin* [1987] suggest that it is possible to investigate large-scale features of seasonal variability of the thermal structure from this set of cruises. Similar conclusions were also attained from model simulations of dynamic height and zonal dynamic topography in *du Penhoat and Gouriou* [1987] and *Reverdin and du Penhoat* [1987].

The procedure to construct a seasonal cycle follows. For each station, the profiles (salinity, temperature, current, oxygen) are interpolated on potential density surfaces. At each grid point (latitude, longitude, isopycnal level), time series are estimated by applying a cubic spline to the available cruises. When a cruise is missing, in order to retain some information on the seasonal cycle, we introduce proxy data corresponding to the same season during the other year sampled. This applies to the currents for the January–February 1983 FOCAL 2 cruise, and for all parameters at 35°W during the October 1983 FOCAL 5 cruise.

There are two sources of uncertainty for the seasonal cycle. One is related to the errors on the data; the other, to the insufficient spatial and temporal sampling. Both are discussed in Appendix B (salinity) and Appendix C (zonal current) and their conclusions summarized below.

The conductivity sensor drifted, and there were insufficient salinity samples to do a station by station in situ calibration. We only remove an average bias. We compare the cruise average T–S with the T–S relationship from a reference cruise (FOCAL 1) for the equatorial waters east of 25°W between 5°N and 5°S. Salinity drift does not depend on temperature between 7°C and 14°C, and is usually quite stationary during the 45 day duration of one cruise. An average correction is applied assuming that it is related to changes in the conductivity cell. According to independent data, the resulting accuracy of the salinity should be of the order of 0.01 (Appendix B1) (in the following, the salinity unit is the practical standard unit). Both in the thermocline and at the surface, errors due to insufficient sampling are larger and often exceed 0.1 (Appendix B2).

The zonal currents are compared to simultaneous mooring data at the equator [*Weisberg et al.*, 1987]. A mean bias is found and corrected (Appendix C1). In the thermocline core, accuracy is better than 10 cm/s, but degrading occurs near the surface. Near the equator, the error on the reconstructed time series resulting from the discrete sampling is of a comparable magnitude (10 cm/s in the thermocline core, 20 cm/s near the surface). The reconstructed seasonal cycle on isopycnal surfaces is reproduced only in places where it is strong, i.e., along 4°W. One questions whether it would have been more accurate to use mooring data for estimating the seasonal cycle on isopycnal surfaces. However, then there are errors associated with vertical resolution which have a similar magnitude (especially at 4°W, see Appendix C2).

Away from the Equatorial Undercurrent, the accuracy of the current profiles is not known but is expected to be better than in the high equatorial shear region. We refer the extra-equatorial profiles to the 475–500 m layer, an approximation which, at the equator, does not lead to a large error.

3. CIRCULATION

3.1. Zonal Circulation

Zonal circulation is constructed from profiler data. The near-equatorial variability is less at 23°W than for the other sections. The most conspicuous features on the average section along 23°W (Figure 2) are also found on individual cruises presented in *Hisard and Hénin* [1987]. *Fahrbach et al.* [1986] showed the association of the EUC core with a salinity and oxygen maximum in 1979 data, and discussed the meridional separation between the salinity and current cores. This is also present here, and the off-equatorial salinities are lower with the thermocline maximum values being less at 3–4°N and 2–3°S than between 0 and 1°S. The salinity and oxygen maximum indicate that part of the EUC waters have been recently advected from the southern subtropical gyre, as is commented in *Metcalf and Stalcup* [1967]. The upper density surfaces bow upward near the equator, and the surface layer (within 1° of the surface temperature) is often shallower there.

Along 23°W, the EUC is located in the thermocline between 1.5°N and 1.5°S. The current extends from the surface layer base down to 250 m. Its maximum velocity near 80 m ($\sigma_\theta = 25.30$, $T \sim 20$°C) is of the order of 80 cm/s and is located between 0° and 0.5°S. This slight displacement of the core south of the equator is more pronounced in the upper layer. In the surface layer, the flow is usually westward, except near 2°S. The subsurface structure is typical of the three longitudes: at 35°W, the EUC is slightly broader, extending to 2°N and 2°S, and maximum velocity is weaker at 4°W (of the order of 70 cm/s near 65 m). The maximum average velocity is also found at a higher density (colder waters) in the eastern Atlantic compared to the western Atlantic.

The EUC mass transport is estimated as the transport of the eastward currents > 20 cm/s below the surface layer. It usually decreases from west to east with values (average and estimate of the sampling error in parenthesis) of 18.2 (1.5), 16.0 (1.1) and 10.2 (0.7) 10^6 m^3 s^{-1} for the three sections, respectively. For the western Atlantic, this is in the same range as other estimates of eastward current transport near the equator. For instance, *Katz et al.* [1981] find 21 × 10^6 m^3 s^{-1} from cruises in 1978–1980 between 20°W and 33°W. This includes a contribution of 1 × 10^6 m^3 s^{-1} by an eastward surface jet. In June–July 1974, the transport in the central Atlantic was 10 × 10^6 m^3 s^{-1} (*Katz et al.* [1979], where the currents were referred to 300 m).

A mean circulation is constructed on isopycnal surfaces by averaging the individual cruises isopycnal estimates. On Figure 3, a meridional average between 1.5°N and 1.5°S which spans the EUC is made as well as a vertical average between a few selected isopycnal surfaces. There is an interesting zonal structure both in density and currents. The isopycnals above 26.4 slope upward to the east, as does the base of the surface layer. On average, the larger velocity

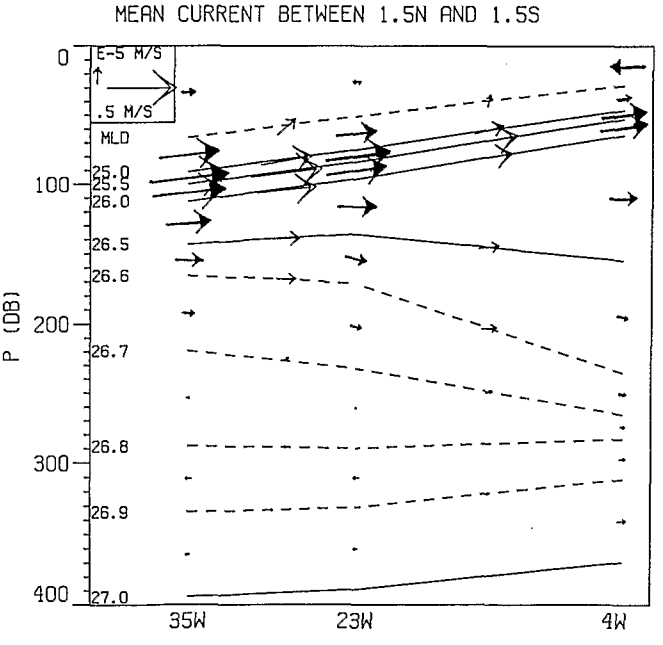

Fig. 3. The 1.5°N to 1.5°S mean circulation along the equator in the FOCAL cruises. The average depth of isopycnals is reported, and the upper dashed line corresponds to the base of the surface layer. The average current within each of the layers is reported at 35°W, 23°W, and 4°W. On isopycnal surfaces between sections, we plot a composite of the isopycnal current along the sections and of the diapycnal velocity between the sections (the velocity scaling in the upper-left corner is equal to the ratio of the zonal and vertical length scale).

is found 35 meters below the surface layer base, i.e. at a density of 25.3 at 35°W and 25.7 at 4°W. Vertical shear between the core and surface layer base is large with average values increasing from 0.0315 s^{-1} at 35°W to 0.0540 s^{-1} at 4°W. In these layers, there is a strong eastward reduction of the EUC transport (for example, between 25.0 and 26.0, from 4.3 × 10^6 m^3 s^{-1} at 35°W to 2.6 × 10^6 m^3 s^{-1} at 4°W).

Below the core, the shear and vertical density gradient are stronger in the west. Also, at all levels, the current in the east is less eastward than in the west. On the other hand, the layer integrated transports between 26.0 and 26.5 (between 17°C and 14°C) do increase from west to east (for example, by 1.8 × 10^6 m^3 s^{-1} between 35°W and 4°W in the layer 26.4–26.5). Below, between 26.5 and 26.6 there is an eastward reduction of speed, but the layers thicken toward the east and the changes in the transports are not significant: 1.8, 1.9, and 1.5 × 10^6 m^3 s^{-1} (35°W, 23°W, and 4°W, respectively). This layer in the east is referred to as the equatorial thermostad [*Katz et al.*, 1979]. Below the thermostad, average currents are more uncertain (large fluctuations compared to the average). The change of the mean zonal slope of the isopcynal surfaces with depth is, however, significant which could suggest a vertical structure of the dynamics. The slopes are null near 270 and 125 m. The structure is also noticeable in the climatology [*Merle*, 1978] and in analyses of XBT sections [*Reverdin et al.*, 1991]. In the FOCAL cruises, the average dynamic height decreases between 35°W and 4°W by 0.7 dyn cm at 270 m referred to 500 m and increases by 1.2 cm at 125 m referred to 270 m. The surface slope referred to 500 dbar is 9.6 dyn cm [*du Penhoat and Gouriou*, 1987].

In the east, large seasonal variations are superimposed on the average current structure presented on Figure 3 (see Figure C3). The vertical (isopycnal coordinate)-time plot (Figure 4*a*) of the 1.5°N–1.5°S average current shows that the current core is denser during the upwelling season than earlier in the year. Its density evolves at the same time as thermocline top density (also demonstrated in *Voituriez* [1981, 1983]). The data also suggest a seasonal cycle in maximum velocity with largest values when the core is the shallowest. The level of maximum salinity located above the current core has a seasonal variability close to the one of the current. However, salinity vertical structure also changes considerably (Figure 4*b*) with maximum salinity being less during the upwelling season (individual sigma surfaces are discussed in Appendix B). The largest salinity is found in early May 1984 with individual profiles maximum salinity > 36.4. This was also found in sections further east [*Piton and Wacongne*, 1985]. There is no clear evidence of seasonal variability of salinity or current below σ_θ = 26.3 (or T = 15°C), the densest surface where the current core was found. Most of these characteristics are shared with the section at 23°W, but the variability of salinity and currents within the thermocline is smaller at 35°W.

3.2. Meridional Circulation

We expect a meridional circulation convergent toward the equator roughly from the surface 26.0 up to the base of the mixed layer from isopcynal slopes (Figure 3) and associated dynamic height gradient. This will contribute to an upward diapycnal transport. The zonal pressure gradient experienced large variability in 1982–1984 [*Weisberg and Wein-*

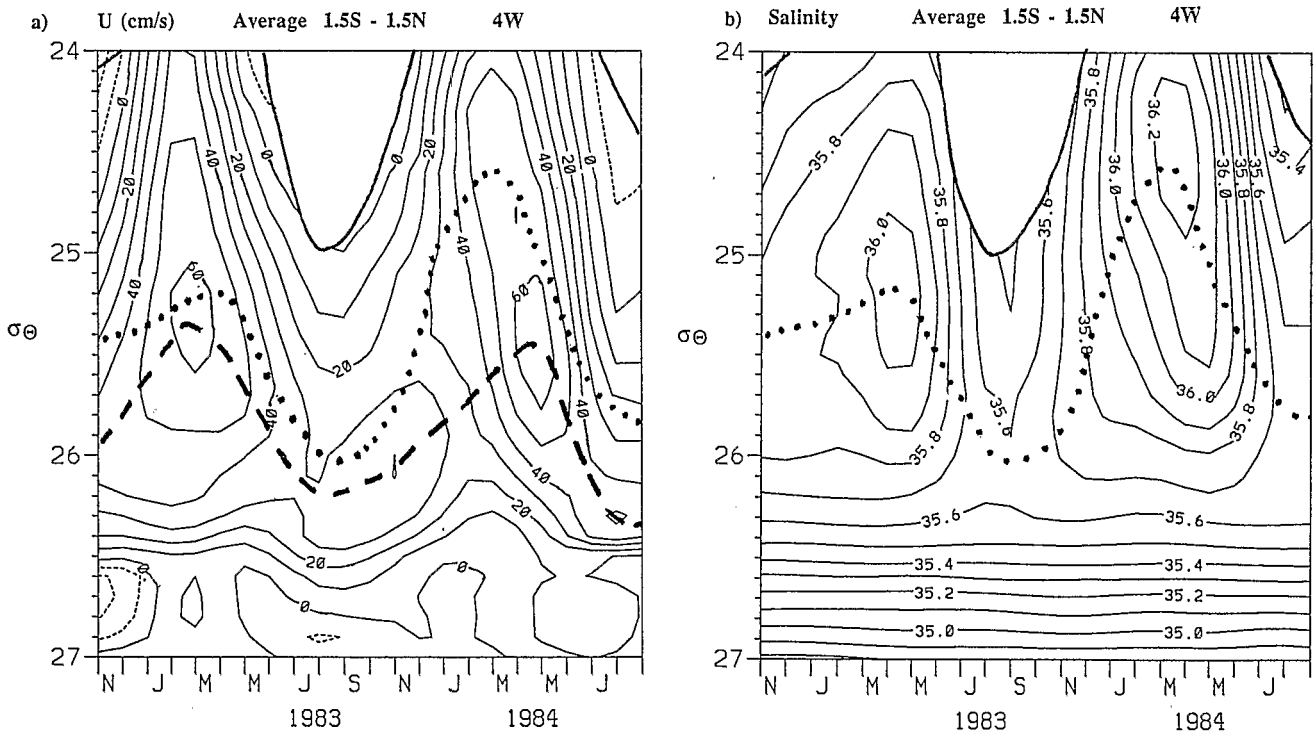

Fig. 4. Current and salinity averaged between 1.5°N and 1.5°S along 4°W are plotted in a time-density plot. Areas within the surface layer have been removed; maximum current is indicated by a dashed line, maximum salinity by a dotted line. (*a*) Zonal current, and (*b*) average salinity.

gartner, 1986; *du Penhoat and Gouriou*, 1987; *Reverdin et al.*, 1991]. Therefore, we could expect the meridional velocity to experience seasonal variability. In this layer, the off-equatorial waters are fresher, which could induce modulation of near-equatorial salinity.

Profilers cannot be used to infer this low-frequency meridional circulation because of the large aliasing related to subseasonal waves [*Weisberg and Weingartner*, 1988]. Therefore, the momentum equation will be used with additional assumptions. Three methods are used. The first method (A) is based on the assumption that off the equator, vertical advection, vertical mixing, and time evolutions are small in the zonal momentum equations. This simplified momentum balance on isopycnal surfaces (σ_θ) is written as:

$$v\left(\left\langle\left(\frac{\partial u}{\partial y}\right)_{\sigma_\theta}\right\rangle - f\right) = -\left\langle\left(\frac{1}{\rho}\frac{\partial P}{\partial x} - g\frac{\partial z}{\partial x}\right)_{\sigma_\theta}\right\rangle - \overline{\left\langle\left(u\frac{\partial u}{\partial x}\right)_{\sigma_\theta}\right\rangle} - \left\langle\frac{\tau^x}{\rho h}\right\rangle Y(h) \qquad (4)$$

where τ^x is the monthly averaged zonal wind stress estimated from ship reports; h is the depth where T = SST − 1°C, SST being the surface temperature; $Y(h)$ is the Heaviside function: 1 above h and 0 below. The brackets denote averages between two sections, and the overbar, the average of all cruises (6 cruises for the western box and 7 for the eastern box). Advection terms are estimated on isopycnal surfaces: zonal advection is averaged over time series. Individual monthly estimates are very noisy due to sensitivity to EUC meridional displacements, the importance of which was first noted in *Düing et al.* [1975].

Close to the equator, there is a latitude where the relative vorticity must be zero. Obviously, the simplified momentum balance in (4) does not hold there, because the right hand side is far from being small (see section 6.2). At 1.5° off the equator, relative vorticity is nonzero and neglecting diapycnal terms is also sensible. However, errors will result from the neglect of meridional advection by subgrid-scale motions. Near the surface at 1.5°N, waves of 10 to 30 day period induce a large meridional transport of zonal momentum $\{\rho\overline{\langle v'u'\rangle}\}$, heat $\{\rho c_p\overline{\langle v'\theta'\rangle}\}$, and presumably, salt $\{\overline{\langle v's'\rangle}\}$ during the upwelling season [*Weisberg and Weingartner*, 1988]. This is associated to meridional fluctuations of the temperature front north of the equator [*Legeckis and Reverdin*, 1987]. Meridional wave transport quickly decreases with depth according to mooring records, but no transport estimate is available for isopycnal surfaces and they are neglected. Another systematic error is u_t neglect which can be significant on a seasonal time scale. In one instance, FOCAL 6 (January–February 1984), meridional velocity was estimated with a different sign for the two domains (35°W–23°W and 23°W–4°W). In this case, we averaged the two estimates.

All terms in (4) are filtered with a running average of weights 1/4, 1/2, 1/4 for neighboring grid points at latitudes $\lambda - 0.5$, λ and $\lambda + 0.5$. Therefore, the discrete form of u_y is $= (u(\lambda + 0.5°) - u(\lambda - 0.5°))/1°$. None of the included terms is negligible in the thermocline above $\sigma_\theta = 26.5$ for the average balance 1.5° off the equator (Figure 5). Zonal advection is smaller in the east, but indicates a significant deceleration of the flow at this latitude in the flow (largest value is $-.04 \times 10^{-6}$ m/s^2 on $\sigma_\theta = 25.5$ at 1.5°S for the western box). Meridional advection has similar values to the Coriolis force; v is half the estimate if meridional advection had been omitted. The zonally averaged u_y is the average of only two sections and exhibit a large variability, resulting in an uncertainty on v. However, in general, the v cycle follows

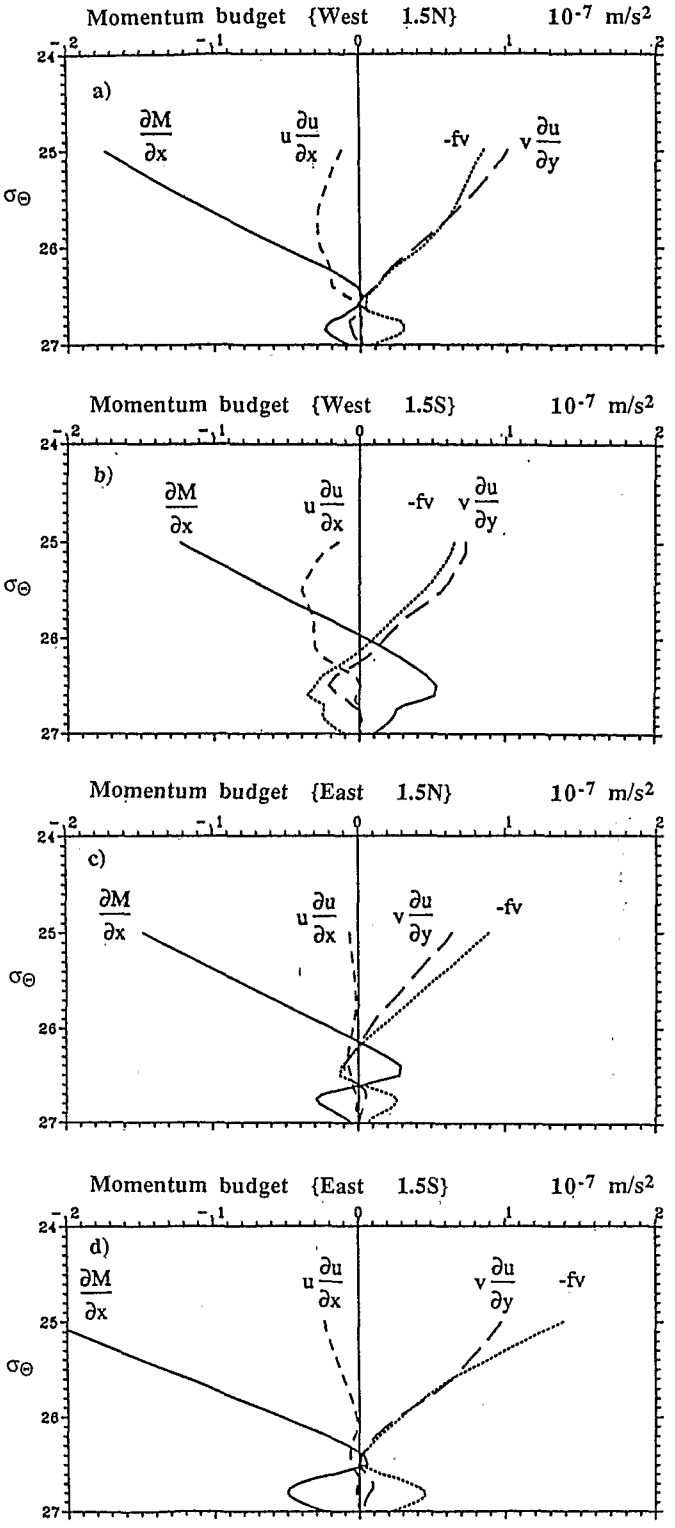

Fig. 5. Average zonal momentum balance at (*a*) 1.5°N and (*b*) 1.5°S below the 25.0 sigma surface for the western box; (*c*) and (*d*) Same for the eastern box. Pressure force, zonal and meridional advection, and Coriolis force are indicated: $\partial M/\partial x$ is $(1/\rho\ \partial P/\partial x - g\ \partial z/\partial x)_{\sigma_\theta}$.

the cycle in the pressure force. Error in the zonal pressure gradient is the main source of random error. The random error on the mean associated with the scatter of the eight seasonal estimates is a large fraction of the average (for example, 55% at 1.5°N at $\sigma_\theta = 25.5$ for the western box). The average v profile (or $\{fv\}$ in Figure 5) varies almost linearly with density above $\sigma_\theta = 26.2$. Values at lower levels are at least a factor of 3 smaller than in the upper thermocline, but can still attain 1 cm/s (in the western box, v has the same sign at 1.5°N and 1.5°S).

Within 3° of the equator, profiles of meridional velocity in the upper thermocline and near the surface are comparable for the "west" (35°W to 23°W) and the "east" (23°W to 4°W). Figure 6 shows a convergence toward the equator in the thermocline and a divergence aloft in the surface layer. Maximum subsurface velocities are on the order of 5 cm/s. Velocity decreases equatorward of 2°N but south of the equator velocity increases between 2°S and 1.5°S. A question is, At what latitude do neglected diapycnal processes become important in the zonal momentum equation so meridional velocity will differ from this estimate?

An independent estimate of v is obtained by integrating meridionally the continuity equation, assuming no vertical motion as in *Bryden and Brady* [1985]. Previously, we attempted the more consistent hypothesis of assuming no diapycnal velocity, instead of no vertical velocity. However, meridional integration on isopycnal surfaces is very large, and this attempt was inconclusive. The computation is therefore carried on depth levels. At the initial latitude, we assume that nonlinear terms and subgrid transports are small, so the subsurface velocity is in geostrophic balance. When an Ekman transport is estimated, it is integrated meridionally by distributing it uniformly through the surface layer (the layer within 1°C of the sea surface temperature).

Two estimates of v are provided depending on how u is estimated: (B) a geostrophic estimate as in *Bryden and Brady* [1985] with an Ekman flow in the surface layer; (C) the currents from the profiler with a reference at 475–500 dbars. There are a few instances along 23°W when the geostrophic zonal current differs strongly from the subsurface South Equatorial Undercurrent near 4°S (Figure 2). This may be due to an insufficient sampling of this very narrow current. In other cases off the equatorial belt, the same features are present in the geostrophic currents as in the profiler currents presented in Figure 2*a*.

Integration starts from 4.5°N and 4°S in the west, from 4.5°N and 4.5°S in the east where meridional transport by waves is neglected. This assumption is supported by *Weisberg and Weingartner* [1988] analysis along 28°W. We also assume at this latitude that v is geostrophic below the surface layers. The meridional sections of v for these two approaches bear similarities with case A, often showing a meridional convergence toward the equator in the thermocline and a divergence aloft. Method C can be integrated to the equator, and expectedly shows a discontinuity there. At which latitude does mass balance without diapycnal velocity break down? According to a numerical simulation discussed in *Wacongne* [1988, 1989], this happens within 1.5° of the equator and the average meridional current varies linearly between 1.5°N and 1.5°S.

It is at the lowest latitude, where methods A and B are used (1.5°N and 1.5°S), that the three methods show

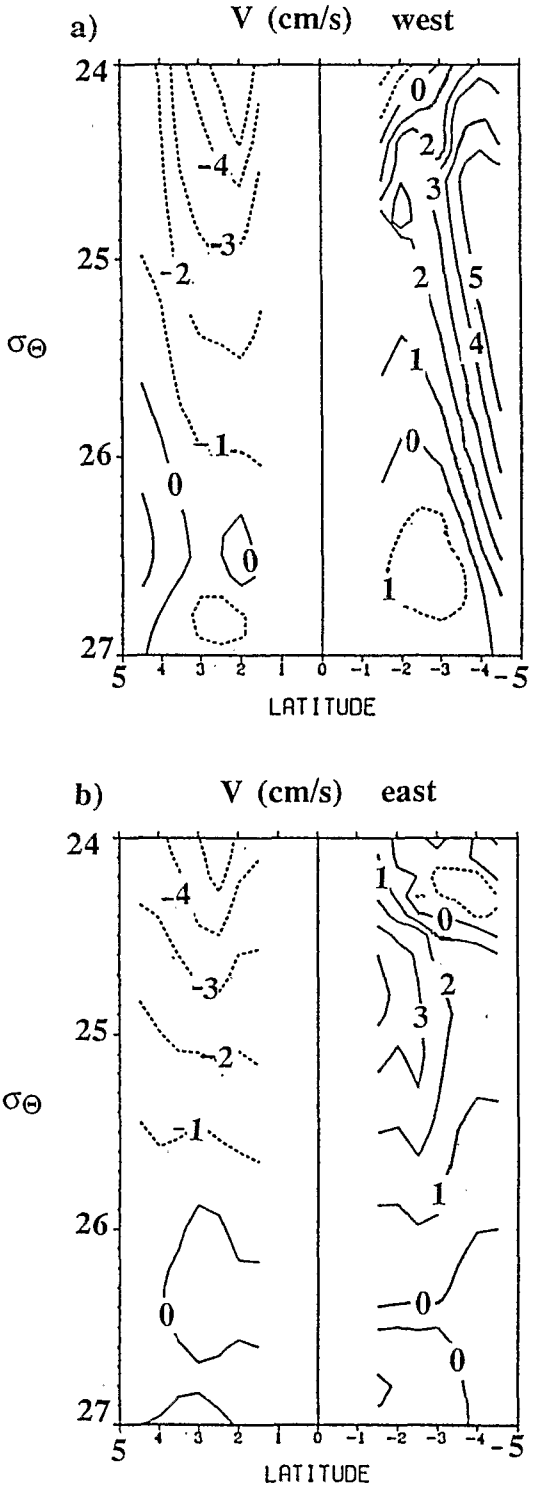

Fig. 6. Meridional sections of the average meridional velocity (sigma coordinate), estimated from the simplified momentum equation (3). (*a*) Western box; and (*b*) eastern box.

the largest differences. The three average profiles of v are presented up to $\sigma_\theta = 25.0$, as well as for layer between $\sigma_\theta = 25.0$, the base of the surface layer and within the surface layer (Figure 7). The three estimates exhibit a similar structure below $\sigma_\theta = 26.5$ in the eastern box, with a meridional divergence near $\sigma_\theta = 26.5$ and a convergence below. Further up, there are large differences between the three so-

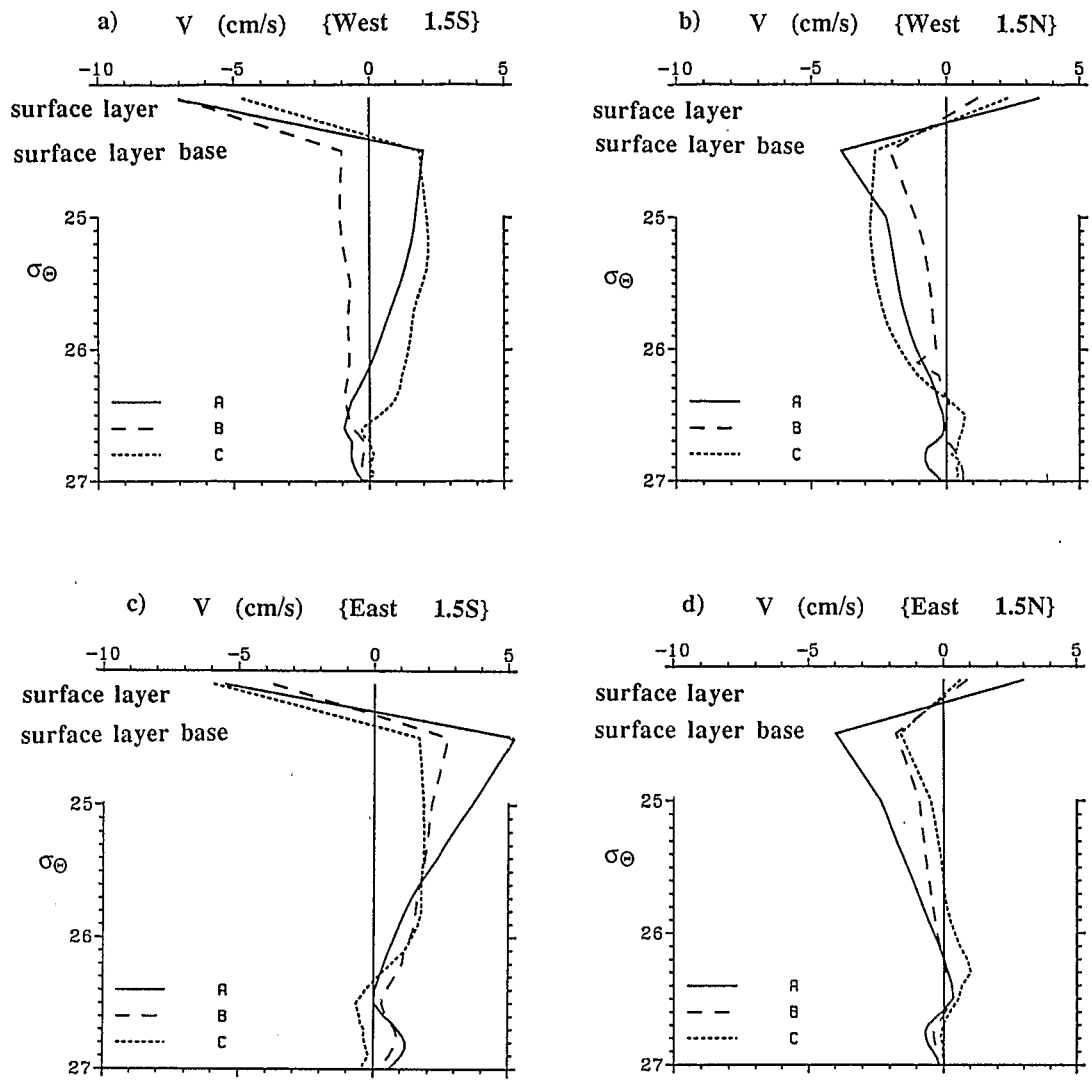

Fig. 7. Average meridional velocity estimated from mass balance by three different methods (method A: eq. (1); methods B and C integration of the continuity equation from meridional boundaries further from the equator, method B with a geostrophic zonal current and method C with the current from the current profiler). The currents are presented below 25.0, in the surface layer and just below the base of the surface layer: (*a*) 1.5°S, western box; (*b*) 1.5°N, western box; (*c*) 1.5°S, eastern box; (*d*) 1.5°N, eastern box.

lutions for v. However, they are not significant at the 95% confidence level, considering the scatter within the set of eight seasonal estimates (with the exception of case B at 1.5°S in the western box with a significantly lower v). It seems systematic however that case B has smaller meridional velocities than the other two cases. The larger v in case A could result from the neglect of zonal momentum meridional transport by waves when estimating case A, in which case B should be preferred, but no reason is found for the difference between case B and case C. Therefore, we cannot conclude what is the best estimate of v.

4. Seasonal Turbulent Fluxes

4.1. Seasonal Salinity Budget

The seasonal variations of mixing will be investigated from the salinity budget (3) applied near the equator, estimating the isopycnal advection with the circulation presented in section 3 and the surveyed salinity fields (Figure 8). There is much structure in the salinity tongue, which exhibits a large spatial and temporal change, not always well resolved in the surveys. To interpret the salinity balance, (3) is zonally integrated between two sections and meridionally averaged between 1.5°N and 1.5°S. Hopefully, this maximizes the diapycnal terms with respect to the neglected transports by horizontal subgrid-scale eddies. The simplified balance is:

$$\int_{1.5°}^{1.5°N} \left(\frac{\partial S}{\partial t}\right)_{\sigma_\theta} + \int_{1.5°S}^{1.5°N} U.\nabla_{\sigma_\theta} S = - \int_{1.5°S}^{1.5°N} DK - \int_{1.5°S}^{1.5°N} \rho_\theta \frac{S_z \dot{Q}_z}{\rho C_p \rho_z} \qquad (5)$$

The last term related to the radiative heat fluxes is estimated from pigment concentration profiles and surface incoming short waves using a spectral model by *Morel* [1988]. The pigment concentrations were measured during four of

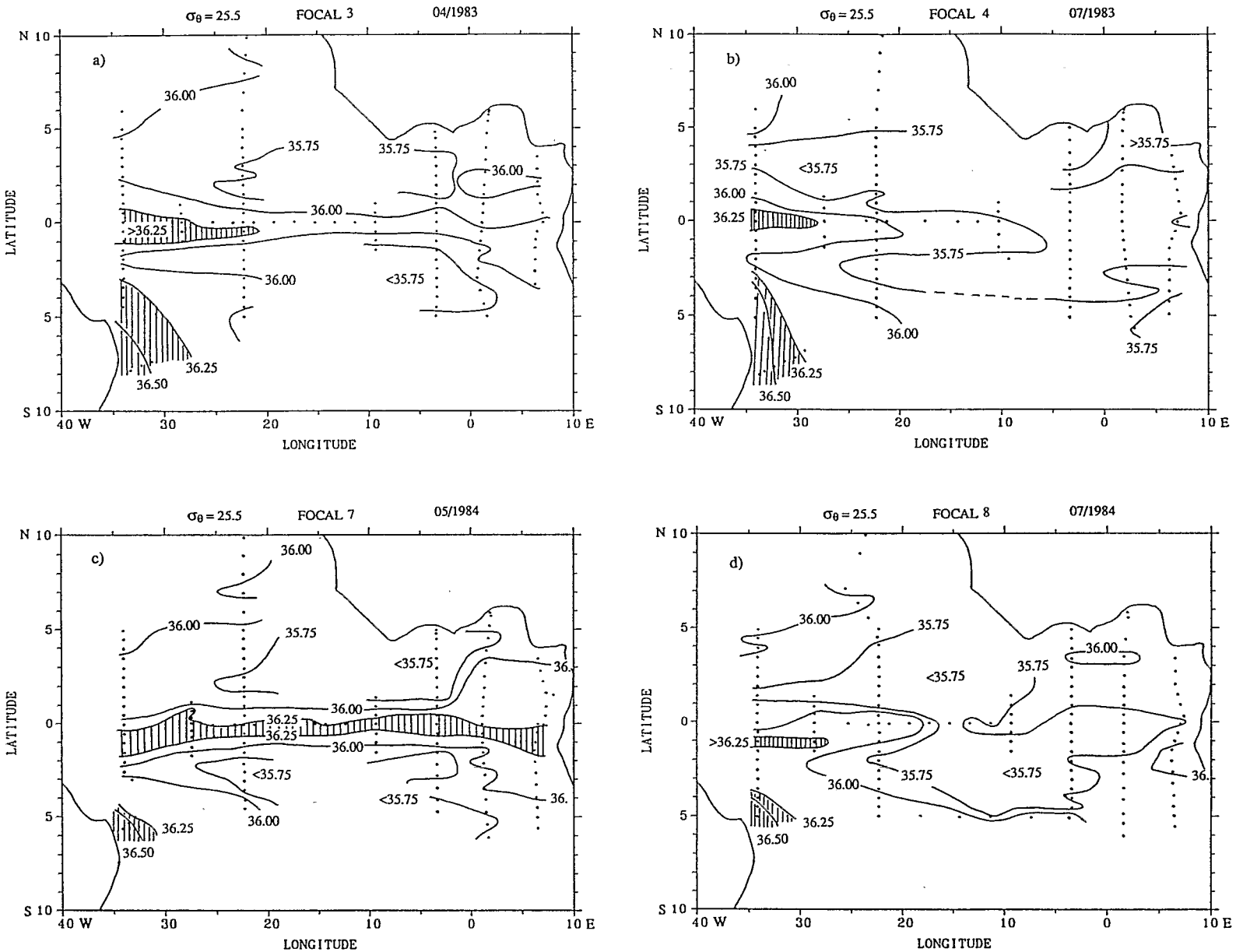

Fig. 8. Salinity on $\sigma_\theta = 25.5$ for four FOCAL cruises.

the eight FOCAL cruises and incoming short waves were deduced between May 1983 an April 1984 from Meteosat data (P. Y. Deschamps and O. Arino, personal communication, 1987). Not obtaining data during the other surveys, we assume that this represents the average seasonal cycle. The radiative fluxes penetrate to denser isopycnals during the upwelling season and contribute to a heating down to $\sigma_\theta = 26.4$ in the Gulf of Guinea (Figure 9). However, the exact values in the upwelling season are strongly dependent on not adequately sampled pigment surface concentration, which often exceeds 0.5 μg/L in that season [*Oudot*, 1988]. On the average, this term is an order of magnitude smaller than the advection terms in the salinity equation, and its magnitude does not warrant further effort.

Time series of dominant terms in the salinity balance (5) are presented for each box (Figure 10). None of the terms is large below 26.20 (expected from Figure 1*b*). In both domains, zonal advection is the largest term. In the west, its cycle is primarily dominated by the cycle in S_x, which is nearly zero in early 1983 and May 1984. In the east, zonal velocity changes also play a role: taking a constant u results in a different cycle. Largest values are also found in the late upwelling season. Temporal variability of S in this eastern box is large with strong negative values of S_t between May and July down to $\sigma_\theta = 26.0$. Most questionable is the linear profile of v used to integrate meridionally the meridional advection (here, case A). However, the budget is not dramatically altered by this choice. For example, if we take $v(1°) = 1.2\ v(1.5°)$, an increase compatible with solution C if there is not diapycnal mass flux, and then v linear between 1°N and 1°S, the meridionally integrated meridional advection is almost twice as large in the upper thermocline. In the western box, even with these larger values the rms meridional advection is only half the rms zonal advection. In the eastern box, meridional advection is smaller because v is large mainly during the upwelling season, at a time when meridional salinity gradients are small: so meridional advection is even smaller than the time derivative of salinity. Therefore, meridional advection is not the reason for the lower salinity in the eastern equatorial Atlantic.

Altogether, both in the west and the east, the left side of (5) (Figures 10*c* and 10*g* represent what could be interpreted as $\int DK$) experiences noticeable seasonal variations above 26.4 with maximum values from mid-May to mid-December 1983 and June 1984 in the west, and in mid-June to mid-October 1983 and May to August 1984 in the east, but where it also remains relatively strong throughout 1983. The seasonal cycle of this term is retained with alternate hypotheses for u or v, although the details of the cycle do change. This budget is done with a three-dimensionally mass conserving circulation (see section 5). However, the results are not very different with a nonconserving circulation, because it is advection which matters, not the divergence of transports in this budget. The sampling error is computed from estimated errors on u, S, and v. For u and S, this originates from the comparison with other data (Appendixes B and C), and for v by estimating errors in the zonal pressure force, considering the subseasonal variance in sea level from tide gauges [*Verstraete and Vassie*, 1990] and assuming that the error diminished in depth as the average profile of the pressure force (Figure 5). The sampling error is estimated on $\sigma_\theta = 25.0$ as 23 and 14 10^{-3} psu m/s for the western and

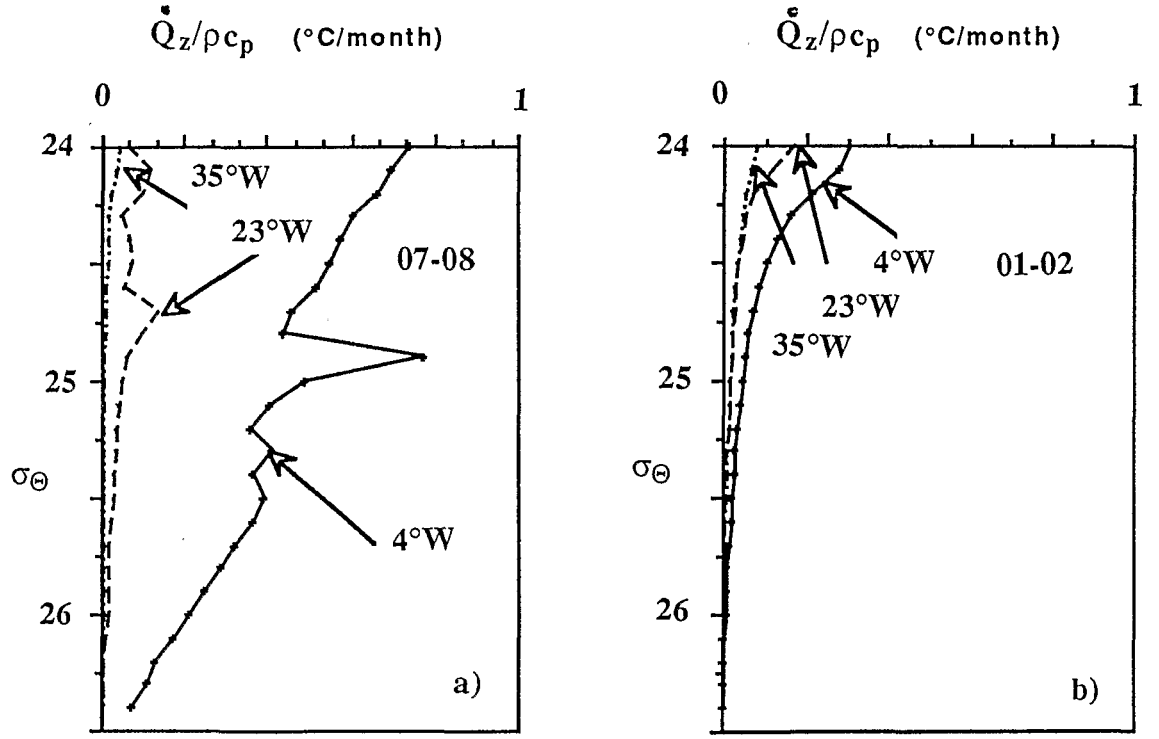

Fig. 9. Near-equatorial heating rate due to the absorption of incoming short waves. The profiles are seasonal averages estimated from *Morel*'s [1988] spectral radiative model and observed profiles of density and pigment concentration [*Oudot*, 1988]. The short waves are from one year of Meteosat data (P. Y. Deschamps and O. Arino, personal communication, 1987), with two seasons presented: (*a*) July–August and (*b*) January–February.

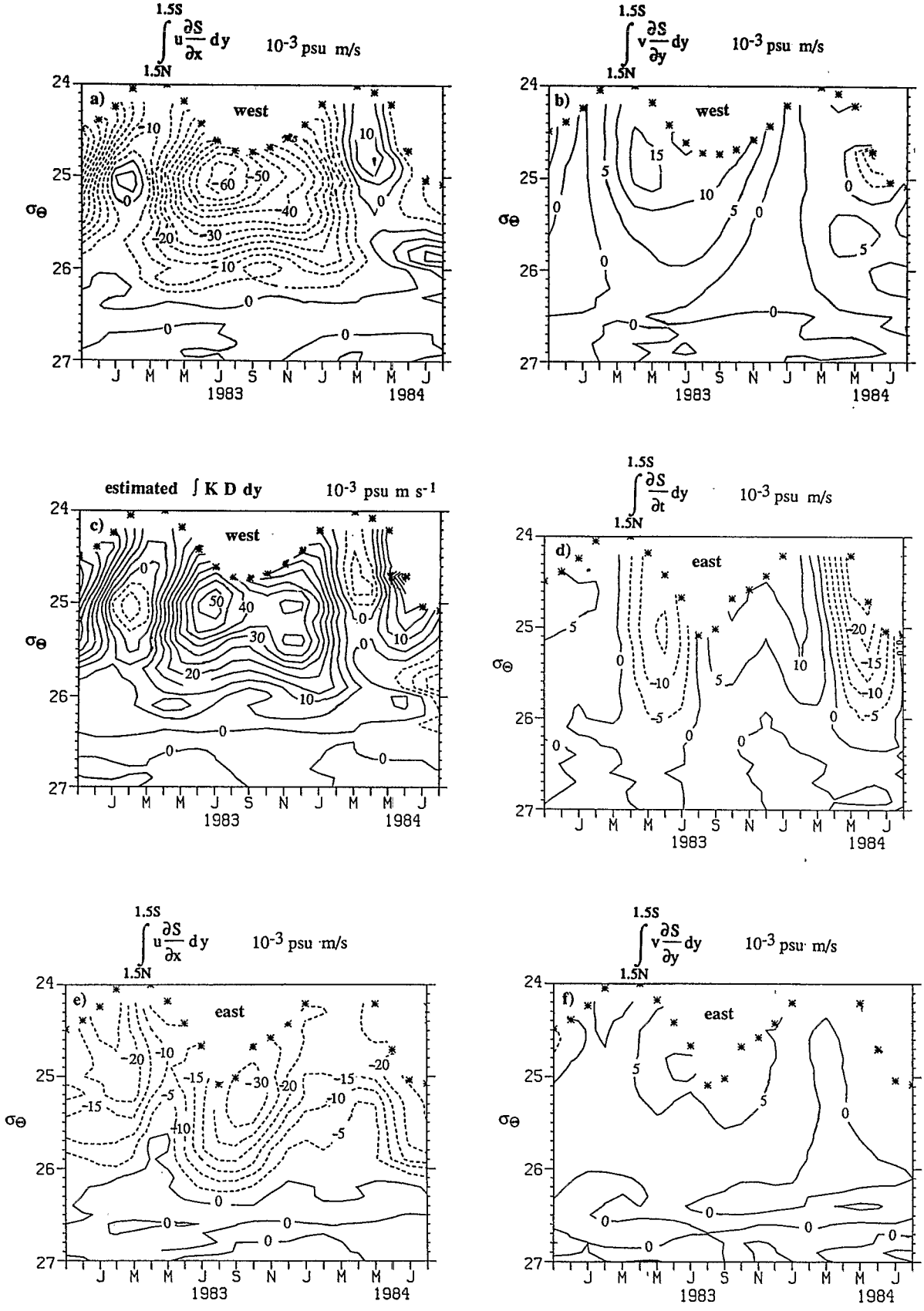

Fig. 10. Dominant terms in the salinity equation (3) for each of the two boxes. Areas within the surface layer or values above $\sigma_\theta = 24.0$ are not evaluated. (*a–c*) Western box: (*a*) zonal advection, (*b*) meridional advection, and (*c*) estimated diapycnal term. (*d–g*) Eastern box: (*d*) Eulerian evolution, (*e*) zonal advection, (*f*) meridional advection, and (*g*) estimated diapycnal term.

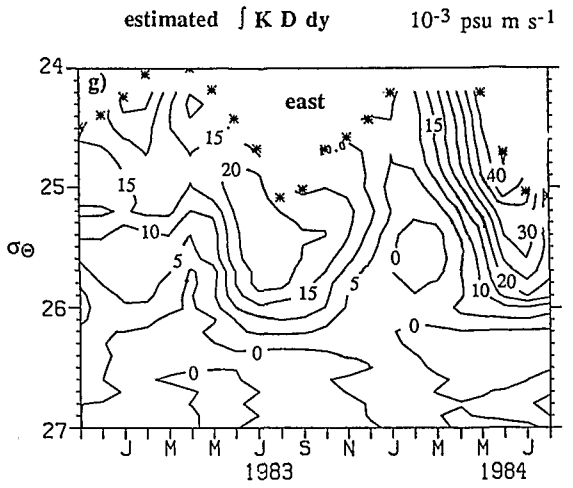

Fig. 10. (continued)

eastern box, respectively, and decreases with depth. It is, fortunately, usually smaller than the seasonal signal. The left-hand side of (2) should be equated to (KD), where D is computed from the θ–S relationship. Above $\sigma_\theta = 25.8$, the curvature in the θ–S diagram (Figure 1*b*) is such that D is mostly positive and the sum in Figures 10*c*, 10*g* should be positive if the balance (5) holds. However, pockets of negative values are found, which can easily be explained by sampling errors.

It is necessary to estimate D to derive the vertical diffusivity coefficient K and therefore heat and salt turbulent fluxes. Individual profiles provide a very noisy estimate of this parameter. For example, the three profiles on Figure 1*b* have very different curvatures in the upper part and errors by an order of magnitude are likely if D is derived from a single profile. Averaging many estimates to obtain reliable values has the disadvantage that it may blur the signal, as some of the profiles are probably not associated with mixing. Because we expect that mixing takes place at the EUC core latitude, we average the three estimates closest to this latitude during each meridional section. As this is still too noisy, we have combined the two years to obtain one seasonal cycle and then combine two sections (35°W and 23°W or 23°W and 4°W) to have a domain average. The seasonal cycle of D (Figure 11) shows high values above $\sigma_\theta = 25.0$ in January–May, and deeper from July to November with a maximum near $\sigma_\theta = 25.2$ for the western box and $\sigma_\theta = 25.7$ for the eastern box. This feature corresponds to the observed density changes of the salinity core (Figure 4*b*). Other details of the cycle are not reliable. The left-hand side of the salinity budget (5) is dominated by zonal advection and therefore S_x. Because a large S_x implies that the θ–S will have a large curvature at a higher density in the east than in the west, where it has little curvature below 25.0 (Figure 1*b*), the seasonal cycle of D and the one in $\{KD\}$ should look alike below $\sigma_\theta = 25.0$. This happens with a tendency for the maximum in D to occur later. In the upper thermocline, the difference between D and $\{KD\}$ is more pronounced.

4.2. Turbulent Fluxes

The seasonal cycle and the vertical dependence of the eddy diffusion coefficient are questionable, even when the domain of computation includes only D larger than 5×10^{-4} psu m^{-2} (Figure 11). This is almost equivalent to retain only values found at and above the EUC core (see Figure 4). In the western box, there are suspiciously large values of K when D gets small, and the field seems more noisy than in the east. Values are small in January–April 1984 and March–May 1983 in both domains. In the east, larger values of K are between July and October 1983 and in June–July 1984, where they reach 2 cm^2/s. In the west, the period May–July 1983 corresponds to the larger values (over 3 cm^2/s where mixing is scaled over a 1° latitude band). The seasonal cycle of the turbulent heat flux $\{-K\rho\ c_p\ d\theta/dz\}$ (not shown) closely follows the one in K.

To find a vertical structure, we average these estimates of K (or the turbulent fluxes) over the 22-month span. Turbulent heat fluxes are shown for the two domains (Figure 12). In the west, the profile is sensitive to arbitrary choices made on whether or not situations with a small D are retained. In the east, fluxes do not exhibit large vertical variations, as was already apparent in Figure 11 for K. Above 25.0, the average only includes some seasons, because of variations in the sea surface density. Indeed, the average turbulent heat flux just below the surface layer (53 W/m^2) is comparable to the flux at $\sigma_\theta = 25.0$. It should be mentioned that Figure 12 only includes values above the EUC core, which experiences large density changes, so that the annual average for the highest densities can be less than indicated if fluxes are small below the core.

To find how sensitive the result can be on the seasonality of D, we also choose D constant in the previous computation. The changes are not large for the average profile, suggesting that it is not too sensitive to errors in the cycle of D. With this approach, we can also estimate the mixing coefficient near $\sigma_\theta = 26.4$–26.5 below the EUC core. At this level, there is an average eastward increase of salinity of 0.03–0.04 between 35°W and 4°W (estimated sampling error of the order of 0.01), which cannot be interpreted from meridional advection or horizontal mixing. The average curvature in the θ–S relationship is sufficiently large to estimate D. The mixing coefficient K is found to be of the order of 0.6 cm^2/s (scaled over 1° of latitude) at $\sigma_\theta = 26.5$ for both boxes. It is less reliable at $\sigma_\theta = 26.4$ with larger values for the western box. The turbulent heat or salinity fluxes implied by these estimates are not very large (4.5 W/m^2 at $\sigma_\theta = 26.5$ close to a depth of 150 m for the average of the two boxes: 3° of latitude and 31° of longitude), because the vertical gradients of T and S are smaller there than further up.

These results suggest that vertical mixing is much less intense below the EUC core than above it. If eddies were transporting properties across the core of the undercurrent, a change related to the fresh upper waters would be expected below the core level. However, the salinity in the EUC core remains close to the largest $S(\theta)$ for the western equatorial Atlantic (Figure 13), suggesting that the eddies which mix the core water with the overlying water do not penetrate below.

4.3. Surface Layer Budget

The surface layer base turbulent heat flux (Figure 14*a*) is estimated by extrapolation from the closest subsurface isopycnal where K could be estimated. This assumes a continuity of turbulent fluxes below the surface layer. This probably also holds here during the upwelling season when

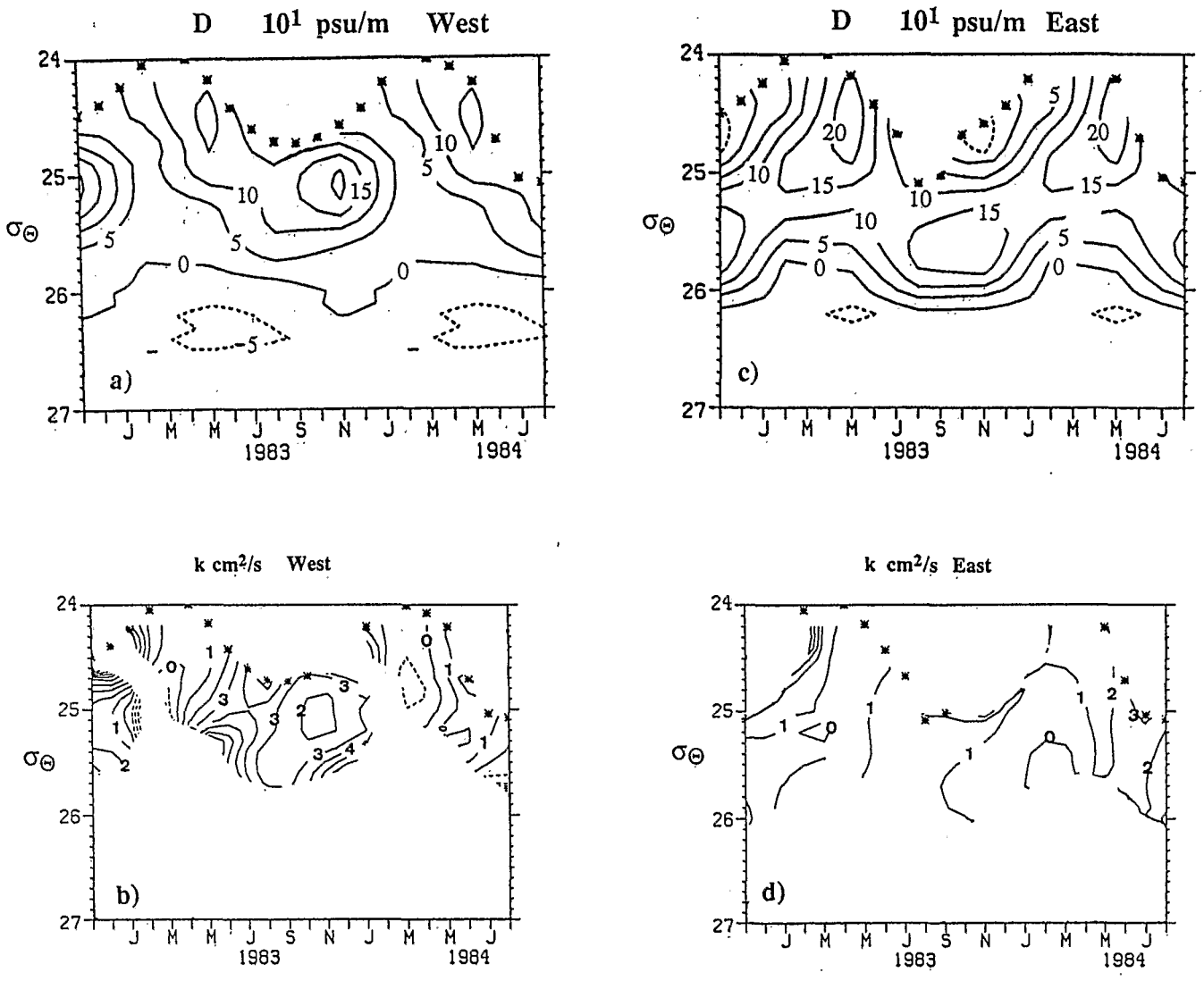

Fig. 11. Coefficient D, and estimation of vertical eddy diffusivity K using (3) for the two boxes. K is shown only when D is larger than 5×10^{-4} psu m^{-2}. (*a*) D in the western box, (*b*) K in the western box, (*c*) D in the eastern box, and (*d*) K in the eastern box.

the surface layer base is not sharply defined, as found on dissipation profiles above the equatorial Pacific Ocean EUC [*Peters et al.*, 1989]. The average turbulent heat fluxes are comparable or larger than the heat flux at $\sigma_\theta = 25.0$ (an average 46 W/m^2 in the west and 53 W/m^2 in the east). A seasonal cycle of the turbulent heat fluxes is suggested which surprisingly has a different phase than the one below (for example, at 25.5 for the eastern box). The large values are associated with seasons where D is small. However, then the estimated fluxes are far from the surface layer base, and the extrapolation of the fluxes to the surface layer base is likely to be associated with large errors.

The heat and salt conservation equations averaged in the surface layer of thickness h, are written as

$$h\frac{D_h\theta}{Dt} + \overline{w'\theta'^b} + \frac{\dot{Q}^b}{\rho c_p} = \overline{w'\theta'^0} + \frac{\dot{Q}^0}{\rho c_p} - h\overline{\langle v'\theta' y\rangle} \quad (6)$$

and

$$h\frac{D_h S}{Dt} + \overline{w'S'^b} = S(E-P) - h\langle v'S' y\rangle \quad (7)$$

the indices b and 0 indicate the base of the surface layer and the sea surface, respectively, Q represents the short wave radiative flux, $\dot{Q}^0$ the surface value, and $\dot{Q}^b$ the surface layer base value (average of 14 W/m^2 in the eastern Atlantic and 5 W/m^2 in the western box). On the right side, the sum of the two first terms in (6) and the first term in (7) represent the surface flux (temperature or fresh water), and D_h/Dt is the operator $\{\partial/\partial t + u\ \partial/\partial x + v\ \partial/\partial y\}$ averaged over the layer depth. We have neglected vertical advection $\{w\partial/\partial z\}$ in the surface layer, because vertical gradients are less there. The meridional velocity is estimated from (3).

The left-hand side sum corresponds to an average heat flux of the order of 58 W/m^2, only slightly more than the turbulent fluxes at the surface layer base (Figure 14*b*). The average left-hand side for salinity corresponds to a fresh water deficit (excess evaporation) of 170 cm/year in the east and 107 cm/year in the west. Ground truth for $E - P$ is only indirectly obtained. During the period surveyed, evaporation computed from ship reports equals 120 cm/year according to *Liu et al.* [1979] (same formulation as *Esbensen and Kushnir* [1981]) and precipitation is estimated as

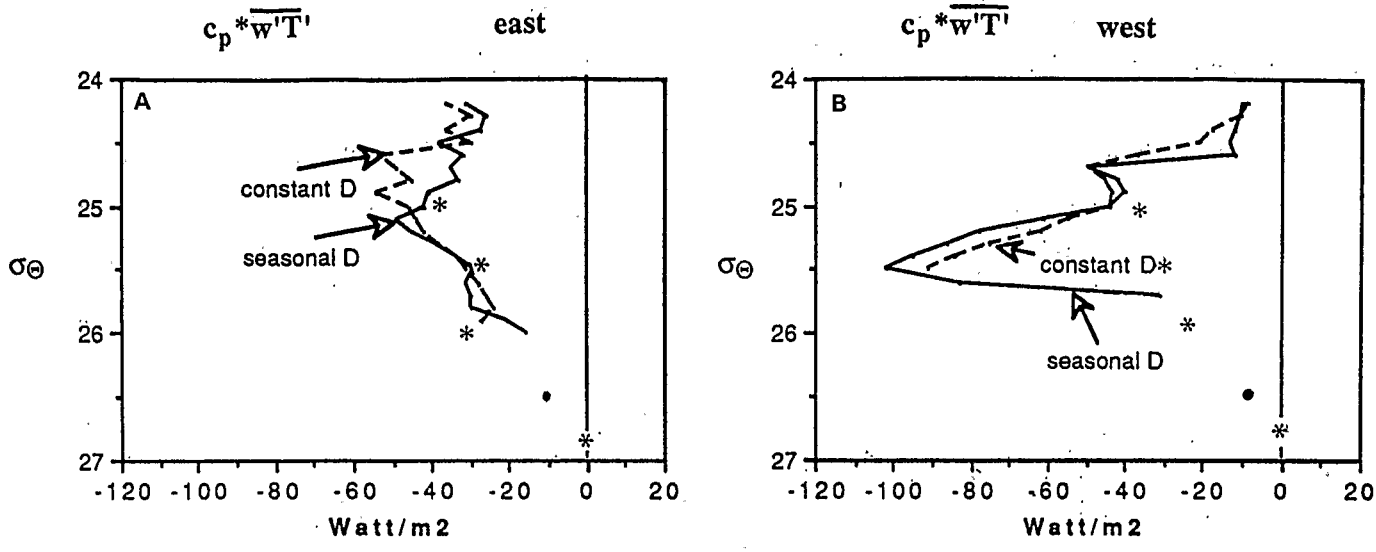

Fig. 12. Average turbulent heat flux for the (a) eastern and (b) western boxes. For layers which surface seasonally, only the subsurface values are included in the average. The solid line corresponds to estimates from (3) with the varying D of Figure 11. The dots at $\sigma_\theta = 26.5$ also correspond to the solution of (3), but with D a constant equal to the 2-year average in Figure 11. The stars correspond to the turbulent fluxes estimated from (2) with the average circulation presented in section 5 and on Figure 4.

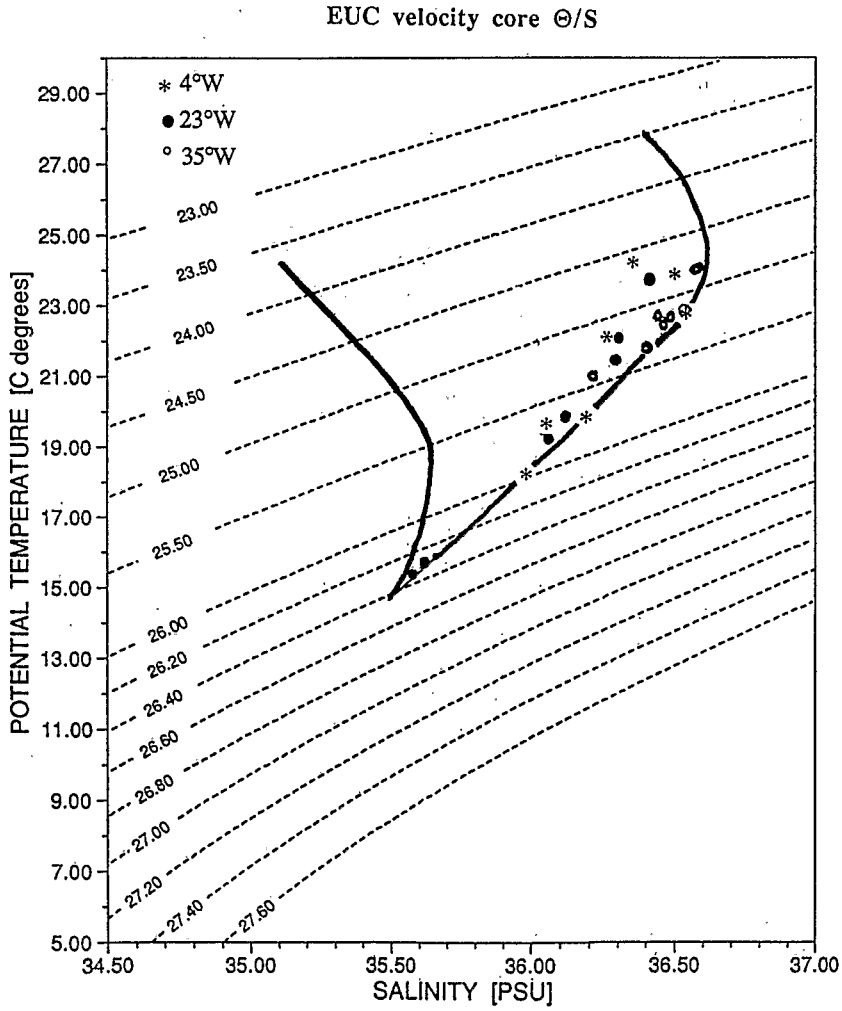

Fig. 13. The θ–S diagram with two curves delineating the range of salinity for the equatorial profiles corresponding to the EUC core. The θ–S values corresponding to the core velocity are indicated (stars) at 4°W, solid dots at 23°W, and open dots at 35°W).

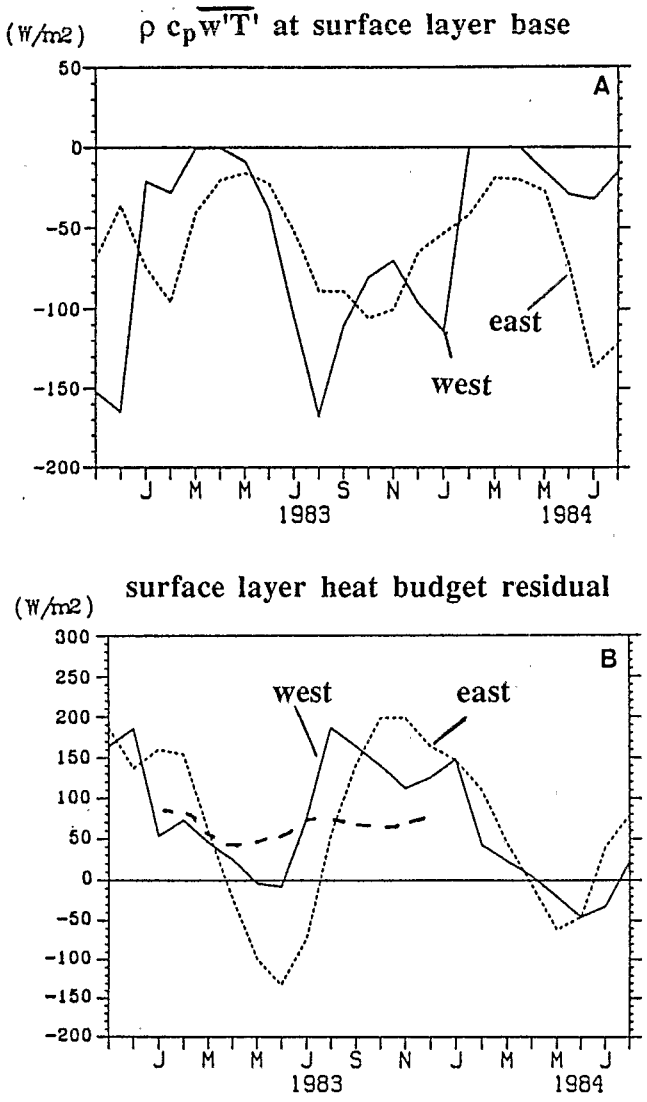

Fig. 14. Surface layer heat budget (6) (dotted line, eastern box, solid line, western box). (*a*) Turbulent heat flux at the base of the layer estimated from the subsurface budget presented on Figure 11 for K. (*b*) Left-hand side of (6). Dashed line is climatology from *Esbensen and Kushnir* [1981].

109 cm/year [*Yoo and Carton*, 1990]. These estimates are in the range of climatological estimates (*Hastenrath and Lamb* [1978] for evaporation; and *Baumgartner and Reichel* [1975] for precipitation), except for larger excess precipitations in February–May 1984, discussed in *Yoo and Carton* [1990]. Although the average heat flux needed to close the temperature budget is realistic according to climatology [*Hastenrath and Lamb*, 1978], the salinity budget is not compatible with the observed fresh water budget at the air–sea interface.

The surface seasonal variability is less well known for salinity than for temperature (Figure B1), a possible source of error, but there are other candidates for this unlikely surface budget for salinity, especially during the upwelling season. One is that the salinity budget is more dependent on meridional processes, either through advection by mean flow or through transports by eddies across the large front north of the equator. Quite suprisingly, we found the estimated turbulent salinity flux to be small during the upwelling season, because $\{\partial S/\partial z\}$ is then small above the undercurrent (Figure 4). This contradicts the following expectation: although the saltier surface waters during the upwelling season originate from upwelling [*Neumann*, 1972], the thermocline freshening should be related to mixing with fresh surface waters, and therefore associated to a large turbulent salt flux. *Fahrbach et al.* [1986] have suggested that the mixing with low-salinity waters occur when the fresh water to the north is displaced southward above the undercurrent. This low-salinity situation above the undercurrent was not sampled during the FOCAL cruises and therefore is not incorporated in flux estimates.

5. Vertical Velocity

Turbulent fluxes estimated in section 4 are too uncertain for reliably deriving diapycnal velocity using (1). Another approach is therefore sought, which is to estimate vertical circulation as a residual of the continuity equation.

The continuity equation is integrated spatially in longitude between two sections (E and W) separated by L_x (average shown by angle brackets) and between 1.5°N and 1.5°S in latitude. The diapycnal transport is then obtained by vertical integration between two isopycnal surfaces 1 and 2 (layer thickness Δz). For the two years' average, $\partial \Delta z/\partial t \sim 0$, so that

$$\left[\int_{1.5°S}^{1.5°N}\left\{\int_{1.5°S}^{1.5°N} u dz\right\} dy\right]_W^E + \left[\left\{\int_1^2 \langle v\rangle L_x dz\right\}\right]_{1.5°S}^{1.5°N} + \int_{1.5°S}^{1.5°N} \langle\{\omega_2 - \omega_1\}\rangle L_x dy = 0 \qquad (8)$$

This equation is applied to the western box (between 23°W and 35°W) and for the eastern box (between 4°W and 23°W) using measured layer transports and estimated meridional velocity. When performing this integration, errors in u or v accumulate producing unrealistic vertical velocities. For instance, if one assumes a 0 diapycnal velocity near 500 m and integrates to the surface in the eastern box with the meridional velocity of method A, the average vertical velocity across the sea surface is larger than 10^{-5} m s^{-1} (or a flux of 5×10^6 m^3 s^{-1}). Although large, this is not significantly nonzero at the 95% confidence level because the spread of individual cruise estimates is large. We are therefore entitled to adjust the profiles without revising the method in order to have a null mass flux across the sea surface. We do that by (1) shifts of the meridional velocity profiles and choices of reference levels for diapycnal velocity, and (2) corrections of v in the surface layer, where v is more uncertain because of the neglected horizontal wave transports and the uncertainty on the wind stress. For example, increasing wind stress by 10% which remains within the unknown on the drag coefficient, results in an increase of surface layer meridional divergence from 8.7×10^6 and 6.4×10^6 m^3 s^{-1} to 10.6×10^6 and 8.1×10^6 m^3 s^{-1} in the western and eastern box, respectively.

In Appendix D, a large range of solutions is presented depending on how v is computed and on the level across which we assume no diapycnal flux. In the following discussion, we add the extra constraint relating to the heat budget that the air–sea heat balance lies within reasonable bounds. For a steady state equation, (2) for temperature is integrated

vertically from the lowest surface (b) where we assume that turbulent heat fluxes are small to the sea surface:

$$\int_0^b \left\{ \left(\frac{d(\theta u)}{dx} \right) + \left(\frac{d(\theta v)}{dy} \right) \right\} dz - (\theta\omega)_b = \frac{1}{\rho c_p} \{SW - L\} \quad (9)$$

The heat exchanges at the sea surface have been decomposed between incoming short waves (SW) estimated from Meteosat data (P. Y. Deschamps and O. Arino, personal communication, 1987) and the other terms (L) which correspond to losses to the atmosphere. We specify a range of 140± 50 W/m^2 for this term within which all the climatologies are found. Because we do not include subgrid-scale heat transports, the equation should be integrated meridionally up to latitudes where the heat transport by waves described in *Weisberg and Weingartner* [1988] is small in a similar way to what is done in *Bryden and Brady* [1985]. In practice, the differences remain within the uncertainties, and we apply the test on the 1.5°N–1.5°S band.

In the west, method A with zero vertical velocity at σ_θ = 26.8 and σ_θ = 27.0 satisfies the conditions on the heat fluxes as well as method B with zero velocities at σ_θ = 26.4 and σ_θ = 27.0. In the east, more solutions give sensible results using methods A, B, or C. The profile of ω (Figure 15) shows an increase of ω toward the base of the mixed layer, and is generally weaker at depth. This increase is related not only to the meridional convergence, but also to the zonal convergence present on Figure 3 above σ_θ = 26.4. There is also a deeper maximum at σ_θ = 26.7 in the west and σ_θ = 26.6 in the east related to the zonal mass convergence in the layer σ_θ = 26.8 to σ_θ = 27.0 (Figure 3). This feature is, however, not significant, given the variability within the set of cruises.

In section 4, we commented that turbulent heat flux is of the order of 10 W/m^2 at σ_θ = 26.5 (125 m). A magnitude for vertical velocity can be associated with it from another form of (1) (derivation in Appendix A):

$$\rho_z \omega = -\{\rho_\theta + \rho_S dS/d\theta\}\overline{(\omega'\theta')}_z - (dS/d\theta)_z \overline{\omega'\theta'}$$

Neglecting this last term, taking $\rho c_p \overline{\omega'\theta'}$ as 10 W/m^2 at σ_θ = 26.5 and 0 W/m^2 at σ_θ = 27.0 and assuming a constant ω corresponds to a diapycnal velocity of 0.2 × 10^{-5} m s^{-1} (scaled over 1°), at least 5 times less than further up in the thermocline. The solutions retained here are often larger at these depths, but not unreasonably so.

Average solutions satisfying the conditions usually correspond to vertical velocities of the order of 2.0 × 10^{-5} m s^{-1} into the mixed layer (assuming a mass flux distributed over 1° of latitude), and of less than 0.5 × 10^{-5} m s^{-1} at σ_θ = 25.0. There is large variability in solutions for individual cruises. Some is expected because of the seasonal cycle: part results from the neglect of layer thickness evo-

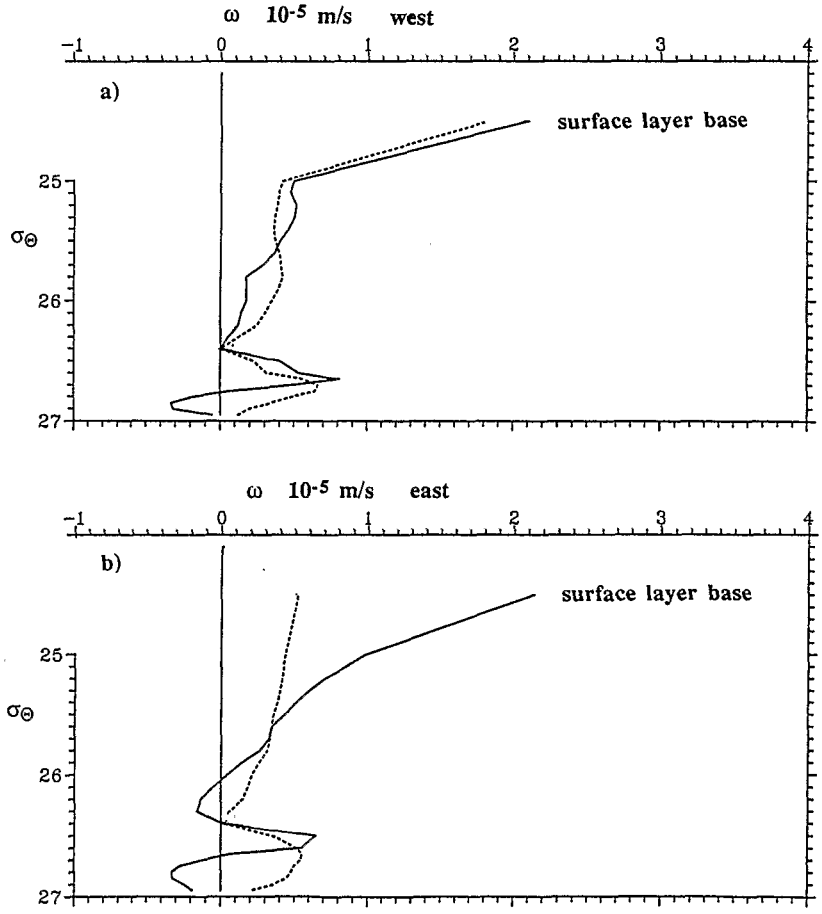

Fig. 15. Method B diapycnal velocity scaled over a 1° meridional band with the additional conditions: ω = 0 at σ_θ = 26.4, σ_θ = 27.0, and at the sea surface. The entrainment velocity into the mixed layer is also shown. Solid line, average velocity; dotted line, rms uncertainty assuming random errors. (*a*) Western box and (*b*) eastern box.

lution in the integration of the continuity equation. Also, some is related to random errors and aliased high frequencies. Assuming as a pessimistic viewpoint, that variability in the set is noise, a sampling error can be estimated. Large values are found in the western box, and few solutions satisfy the surface heat flux condition. in the eastern box, it is smaller than the average surface layer base and upper thermocline heat fluxes and most solutions satisfy the condition on the surface heat flux. This may suggest that the not-so-good adjustment on the surface heat flux in the west is related to larger noise.

The corresponding circulation with isopycnal and diapycnal velocity components has been plotted for a few selected isopycnals in a x–z plane (the thin arrows) in Figure 3. It is interesting to note that at $\sigma_\theta = 25.0$ in the shear zone above the EUC core, the diapycnal component is smaller than the vertical component of the isopycnal flow related to the zonal slope of the isopycnals by factor 2. Below, down to $\sigma_\theta = 26.5$, average vertical velocity for this solution is largely the isopycnal component. For example, at $\sigma_\theta = 25.5$, the vertical isopycnal flux between 35°W and 4°W is 4.8 $\times 10^6$ m^3/s compared with an estimated diapycnal flux of 0.55 $\times 10^6$ m^3/s.

To estimate total vertical flux into the mixed layer, we assume that no transport occurs west of 35°W, but include the influx for the Gulf of Guinea east of 4°W. This influx is known to happen further south than 1.5°S [*Voituriez*, 1983], and another approach is necessary there than the one just described. For this, we will close a box bounded in the west by the 4°W section (the profiler currents are used), in the north by the coast, and in the south at 4.5°S by geostrophic currents estimated from stations at 4°W, 1°E, and 6°E (Figure 16*a*). Southward velocity computed between 1°E and 6°E at 4.5°S is also retained for the unsampled segment to the east. Doing this, we presumably neglect the coastally trapped current described in *Wacongne* [1988]. Peak velocities near the shelf edge are on the order of 8 cm s^{-1} between 50 m and 200 m in January–May, but not statistically different from 0 in other seasons.

Diapycnal velocities obtained with these assumptions are similar to estimates for other domains at the $\sigma_\theta = 25.0$ surface or below (Figure 16*b*). The average influx into the mixed layer is smaller (1–1.5 $\times 10^{-5}$ m s^{-1}, scaled over a 1° wide latitude band), though we have no real basis to validate this estimate. Other solutions produce larger diapycnal velocity. Together with the two other domains,

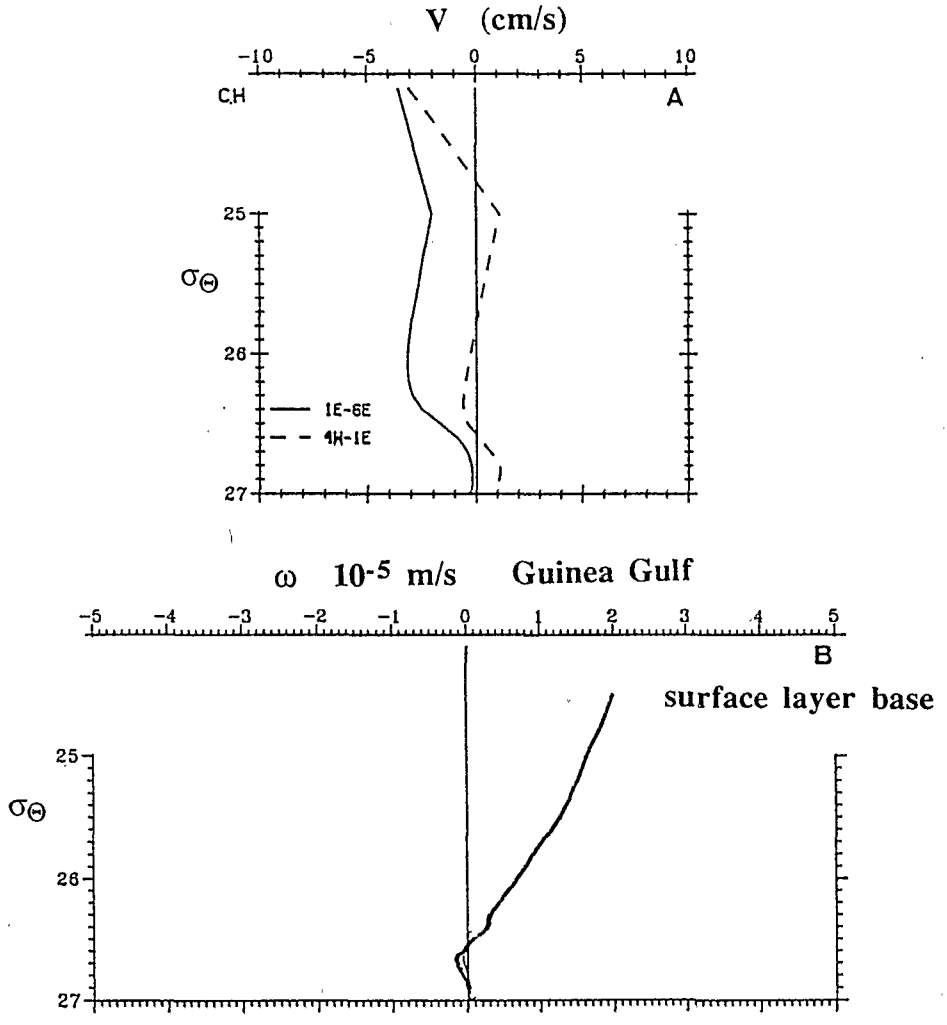

Fig. 16. Circulation in the eastern Gulf of Guinea from hydrographic data. (*a*) Meridional velocity estimated from geostrophy at 4.5°S between 4°W and 1°E, and between 1°E and 6°E (has been extrapolated to the African coast). (*b*) Corresponding vertical velocity for different assumptions on the reference level.

we find an influx into the surface layer of 10.6–14.7 × 10^6 m^3 s^{-1} for the entire equatorial Atlantic, and of 5.2–8.5 × 10^6 m^3 s^{-1} across $\sigma_\theta = 25.0$ (Table 1), and of the order of 1 × 10^6 m^3 s^{-1} across $\sigma_\theta = 25.5$ (temperature between 21°C to 19°C from west to east).

6. DISCUSSION

6.1. The Turbulent Fluxes

Two methods have been used to estimate diapycnal processes with the same data for 1982–1984, one based on a mass budget to estimate the diapycnal velocity and the other based on (3) to estimate a vertical mixing coefficient and heat and salinity turbulent fluxes. As mentioned earlier, there should be consistency between the two estimates: using the diapycnal velocity estimated from the continuity equation, it is possible to compute turbulent fluxes by writing the conservation equation of temperature or salinity in flux form (2). Some of these estimates are indicated in Figure 12. They are very sensitive to ω, for which there is a large uncertainty with values depending strongly on the method used to compute meridional velocity and on the reference levels. There is an encouraging agreement between the two methods in the eastern domain, where the solution is more robust. These indirect estimates of $\{\rho\, c_p \overline{\omega'\theta'}\}$ decrease with depth, in concert with what is expected from microstructure. For the western box, where the choice of ω is strongly constrained by surface heat fluxes, the profile is also comparable to the eastern box but differs from the analysis based on the salinity equation. This suggests that less confidence can be given to this result.

Another estimation of diapycnal mixing is provided by *Katz et al.* [1979], who performed a salinity budget of the EUC. This was based on one cruise in June–July 1974 sampling the zonal structure at six longitudes. This budget was carried by considering the salinity anomaly with respect to a background off-equatorial salinity profile which did not require estimating a meridional velocity. From the 1982–1984 data, it can be argued that the neglect of the time evolution is a draw-back to this approach, at least in the eastern part of the basin. Another approximation which does not seem to hold well according to our analysis, is the neglect of vertical advection at the top of the layer considered ($\sigma_\theta = 24.4$) (the salinity is larger at the equator than at off-equatorial latitudes). Nonetheless, the eddy coefficient of 3 × 10^{-4} m^2 s^{-1} scaled over 1° of latitude above the EUC core [*Katz et al.*, 1979] corresponds to ours for the upwelling season. Below the EUC ($\sigma_\theta = 26.4$), they estimate a heat eddy coefficient of 2 × 10^{-4} $m^2 s^{-1}$ which is larger than ours. However, they consider the salinity zonal gradient in the pycnostad instead of one on isopycnal surfaces. From 35°W to 10°W, they report an increase in pycnostad salinity of 0.20, much larger than the increase on $\sigma_\theta = 26.4$ is of the order of 0.03, which should be used for this budget.

Upper thermocline turbulent fluxes were estimated in *Niiler and Stevenson* [1982] from analysis of air-sea heat exchanges. This study suggests a turbulence heat flux of 140 W/m^2, assuming that turbulent heat fluxes are distributed over 3° of latitude. In the upper equatorial thermocline, our estimate is smaller (50 W m^{-2}). *Reverdin* [1984] pointed out that *Niiler and Stevenson*'s [1982] estimate does not consider the seasonality of upwelling. It could also be that this estimate is uncertain because of the possible biases in the heat flux formula. Indeed, an average error in the air-sea heat fluxes of only 8 W m^{-2} in the tropical Atlantic, well within the error bars, would wipe out the expected turbulent fluxes from this budget.

Although turbulent fluxes in the equatorial thermocline are not dramatic, in the sense that water does not pop up from great depth to the surface, they are still significant, fully modifying the shape of the upper thermocline θ–S relationship as the water drifts eastward along the equator. This happens only during the upwelling season (Figure 8). It might also happen along the African margin and at other latitudes, thereby explaining the disappearance of salty water which spreads off the equator in the Gulf of Guinea during the first months of the year (a discussion of entrainment in the surface layer of the Gulf of Guinea is given in *Houghton* [1989]). Equatorial thermocline water in the eastern Atlantic has comparable salinity in July–August to water found during all seasons in the central Atlantic off the equator (Figure 8), and therefore can be thought to be the source of these low-salinity pools fed by the off-equatorial westward currents (Figure 2). Most of these waters are reentrained later in the EUC through meridional circulation (Figure 7).

6.2. Momentum Mixing

If there is vertical mixing of temperature and salinity, momentum turbulent fluxes are expected. We said that zonal momentum balance (3) without diapycnal terms breaks down near the equator (the unbalanced pressure force remains strong, Figure 5). To investigate momentum turbulent fluxes, we average the momentum equation over the 1.5°N–1.5°S band on isopycnal surfaces as

TABLE 1. Diapycnal Transports (10^6 m^3/s) in the Equatorial Atlantic East of 35°W

	$\sigma_\theta = 26.4$			$\sigma_\theta = 26.8$			$\sigma_\theta = 26.9$		
v	A	B*	C	A*	B	C	A	B	C
Into surface layer	13.3	10.6	13.1	14.7	15.7	15.9	18.5	18.8	17.8
Across $\sigma_\theta = 25.0$	5.2	5.2	6.7	8.5	9.7	9.0	9.9	12.7	10.8
Across $\sigma_\theta = 26.5$	2.0	1.6	1.3	2.4	4.7	2.6	5.3	7.1	4.2

Here, v is estimated using methods A, B, or C described in the text. In all instances, $\omega = 0$ on $\sigma_\theta = 27.0$ and on another surface (for the Gulf of Guinea, the smaller of two solutions is included).
* Solutions for which the surface and subsurface turbulent heat fluxes are realistic (method A with $\omega = 0$ at 26.8 is suspicious in the west).

$$\overline{\overline{\frac{\partial u}{\partial t} + u\frac{\partial u}{\partial x} + v\left(\frac{\partial u}{\partial y} - f\right) + \omega\frac{\partial u}{\partial z}}} = \overline{\overline{-\frac{1}{\rho}\frac{\partial P}{\partial x} - g\frac{\partial z}{\partial x}}} - \overline{\overline{\frac{\partial u'w'}{\partial z}}} + R \qquad (10)$$

where the double overbar indicates

$$= \frac{1}{L_y}\int_{1.5S}^{1.5N} \{\ \}dy$$

and R refers to the mesoscale eddies momentum flux divergence. Vertical advection is computed with the vertical velocity of section 5. We assume that diapycnal processes happen only at the EUC core latitude (as was assumed for salinity mixing in section 4). Consistently with this assumption, momentum vertical advection also happens at this latitude.

The budget is done seasonally from the estimated time series of pressure force (noted for simplicity as $\partial M/\partial x$), u, v, and ω. Similar to the procedure in section 5, for the salinity budget, we assume that v varies linearly between 1.5°S and 1.5°N. This possibly underestimates vorticity meridional advection; however, this term is smaller than the others, except near 26.0 in the eastern box and near 25.0 in the western box. The diapycnal velocity time series are constructed from the integration of the continuity equation for individual cruises. The error on vertical advection is very large for individual seasons (at least a factor 2). We therefore only present the average budget for 22 months.

Above the EUC core, both vertical and zonal advection contribute to a negative left-hand side which is only partially compensated by the meridional advection positive contribution. The left-hand side $\{du/dt - fv\}$ as well as the average pressure force $\{-\partial M/\partial x\}$ are presented in Figure 17. The difference between the two terms is large above $\sigma_\theta = 26.2$ in the east and $\sigma_\theta = 26.3$ in the west. It does exceed 10^{-7} m s^{-2} above $\sigma_\theta = 25.6$ in the west and $\sigma_\theta = 25.7$ in the east, then the difference becomes much larger, reaching 3×10^{-7} m s^{-2} near the mixed layer base.

This concurs with the assumption that deceleration due to mixing is stronger above the core, although in the west there is a relatively large difference between the two curves below the core (the core is always above 25.6). If R is negligible and the fluxes are related to the local shear as $\overline{u'\omega'} = -K_m u_z$, $-\partial\overline{u'\omega'}/dz = K_m u_{zz} + (K_m)_z u_z$, deceleration at the core level implies either a nonzero K_m or that the core is a cusp in the velocity profile with a large velocity gradient and $(K_m)_z$ above it. This does not contradict the suggestion from microscale measurements that turbulent fluxes are small at the core. Assuming $\overline{u'\omega'} = 0$ at the core and $R = 0$, (10) can be integrated upward from the core of the EUC to estimate K_m. It would be better to do it seasonally because of changes in core density, but for a first approach, we consider the average situation. At the depth of the strongest vertical gradient, located 30, 27, and 21 m above the EUC core at 35°W, 23°W, and 4°W respectively, K_m equals $\{7.5, 5.1\} \times 10^{-4}$ m^2 s^{-1} for the western and eastern box. $(K_m)_z$ is also large (1.5×10^{-5} m s^{-1}), and the vertical momentum diffusivity is larger close to the mixed layer base. Microstructure estimates of K_m are also in this range. In the Atlantic EUC, *Crawford and Osborn* [1979*b*] find 8×10^{-4} m^2 s^{-1} at 28°W in July 1974; with October 1984 profiles in the equatorial Pacific, *Peters et al.* [1988] find an average K_m of 5–6 $\times 10^{-4}$ m^2 s^{-1} at 50 m.

According to *Osborn* [1980], and used by *Moum et al.* [1989], it is possible in the equatorial thermocline to relate the momentum eddy diffusivity to the heat eddy diffusivity, as $\{K_m = 5\ R_i K\}$, where R_i is the Richardson number. If the mixing episodes associated with most of the momentum transport correspond to near-critical Richardson number, say 0.3, values commonly observed above the Atlantic EUC core [*Voituriez*, 1981], we expect $K = \{5.0, 3.4\} \times 10^{-4}$ m^2 s^{-1}. This value is twice as large as what is found in the salinity budget, although well within error bars.

This finding would suggest that small-scale mixing could explain the momentum budget residual. Studies for the equatorial Pacific reach somewhat different conclusions. *Dillon et al.* [1989], using microstructure estimates of K_m, suggest that momentum vertical eddy transport is not sufficient to close the momentum balance. However, they do not use simultaneous estimates of the horizontal pressure force. *Wilson and Leetmaa* [1988] analyze a set of equatorial current and density sections in the eastern Pacific to establish the upper ocean momentum budget. They estimate turbulent fluxes as a residual from the budget. Their

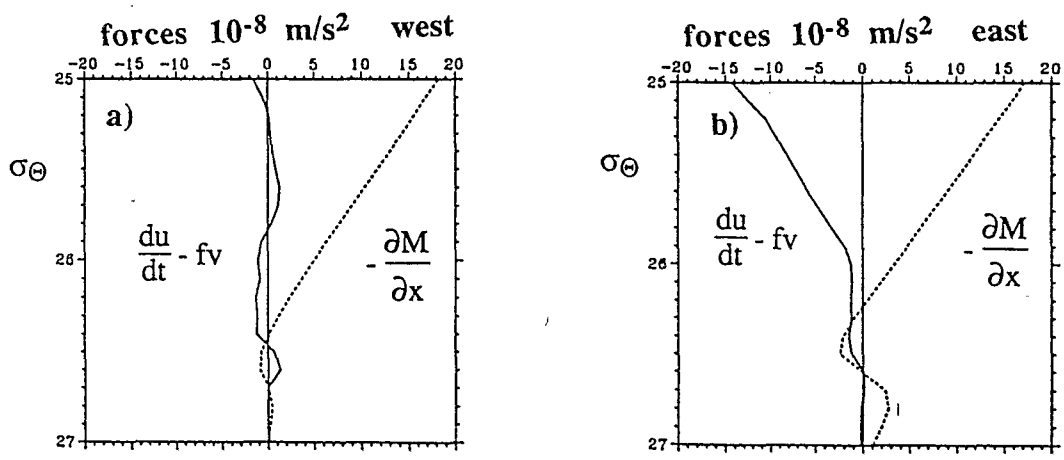

Fig. 17. Average momentum balance (1.5°N–1.5°S) in the two boxes. The average pressure force is shown (solid line) as well as an estimate of the left-hand side (Lagrangian acceleration and Coriolis force).

eddy velocity coefficient between the base of the mixed layer and the undercurrent core averages 8×10^{-4} m^2 s^{-1}. The vertical eddy transport of momentum is a very important term in that layer. However, they also show that there is an important meridional transport of momentum by waves.

Waves which could play a similar role are found in the Atlantic. Surface cusps are seen on satellite imagery of the sea surface temperature front north of the upwelling zone, particularly west of 10°W [*Legeckis and Reverdin*, 1987; *Steger and Carton*, 1991]. Near the surface the waves are found to contribute to meridional heat transport (*Weisberg and Weingartner* [1988] for 28°W and *Houghton and Colin* [1987] for 4°W). However, *Weisberg and Weingartner* [1988] suggest that at 28°W, Reynolds terms are small near 60 m or below and that large eddy transport of zonal momentum is unlikely to be important at EUC core level. By integrating vertically all known terms of the momentum balance (10) upward from the level where $\{-\partial M/\partial x\}$ crosses $\{du/dt - fv\}$ on Figure 17, we estimate $\int R\, dz$. This level is at 26.4 for the western box and 26.2 for the eastern box. There is compensation within the wind stress uncertainty between the wind stress and the other terms (-0.41, -0.32) $\times 10^{-4}$ m^2 s^{-2} for the western box, (-0.18, -0.16) $\times 10^{-4}$ m^2 s^{-2} for the eastern box. This does not suggest a large contribution for waves in zonal momentum balance.

6.3. Upwelling in the Surface Layer

The main result of the study is that transport into the Atlantic Ocean surface layer (through the level at which T = SST− 1°C) is much greater than diapycnal transport for deeper isopycnals (Table 1). Therefore, we expect that cold tongue waters during seasonal upwelling originate from shallow isopycnals. To scale this, we adopt an analogy to the mixed layer approach where the heat budget of the water entrained in the surface layer (average entrainment velocity ω) is

$$\omega \Delta\theta = -\overline{(\omega'\theta')}$$

where $\Delta\theta$ is the temperature jump across the surface layer base. If we distribute the upwelling flux over the domain (3° wide, 40° longitude band) over 6 months, it corresponds to 23×10^6 m^3 s^{-1}. Together with the estimated turbulent heat flux of 100 W m^{-2}, we find $\Delta\theta = 1.5$°C. This suggests that seasonal cooling > 5°C and salinity increase during the upwelling season is mainly the result of the thermocline uplift and the progressive entrainment of thermocline water in the surface layer.

The 23×10^6 m^3 s^{-1} influx into the surface layer during the upwelling season is large compared to the surface layer South Equatorial Current westward transport which averages 12×10^6 m^3 s^{-1} during the upwelling season at 23°W (layer depth averaging 60 m) and is less at 35°W. If this upwelled mass remained in the surface layer within 5° of the equator, this would cause a 65-m averaged surface layer deepening over 6 months. This is large compared to the seasonal vertical displacements of mixed layer depth [*Hastenrath and Merle*, 1987] and illustrates the large seasonal mass divergence from the equatorial zone. It is also possible that the upwelled waters are partially downwelled in the upper thermocline at the temperature and salinity front north of the cold tongue.

The average net heat input from the atmosphere needed to balance the surface layer temperature budget is 60 W m^{-2} for a 3° wide equatorial band for the budgets of section 4 and section 5. Estimated air-sea heat exchanges are in this range with 50 to 60 W m^{-2} in *Hastenrath and Lamb* [1978] and *Hsiung* [1986] and close to 60 W m^{-2} in *Esbensen and Kushnir* [1981]. The average salt budget into the surface layer is, however, less easy to balance. In section 4, the surface layer advective salt budget implied a fresh water loss exceeding 100 cm year^{-1}. We suspect that we strongly underestimate the effect of the salt influx from the thermocline in this budget. Alternatively, an estimate with the three-dimensional circulation presented in section 5 is obtained by vertically integrating the salinity transports in (2) (similar to the temperature budget). We find an imbalance requiring a fresh water input of 85 cm year^{-1} for the 1.5°N–1.5°S band. The 1.5°N–4.5°N band budget requires a fresh water loss. These residuals opposed to climatology expectations could result from erroneous salt transports across 1.5°N, where an intense salt front is present.

The best choice for annual averaged upwelling in the surface layer is 11–12 $\times 10^6$ m^3 s^{-1} with a relatively large range related to the uncertainty of the method and to limited sampling (Appendix D). Other estimates have been published for upwelling in the equatorial Altantic. *Wunsch* [1984] uses an inverse model to estimate upwelling across $\sigma_\theta = 26.5$. He finds 7–10 $\times 10^6$ m^3 s^{-1}, which is larger than our budget (Table 1), but includes a larger area. *Broecker et al.* [1978] and *Broecker and Peng* [1982] estimate upwelling into the surface layer based on the observed near-equatorial surface water deficit in 1972 of bomb radiocarbon compared to the subtropical gyres. The mechanism considered is flush of the surface layer by thermocline waters having less radiocarbon (in 1972, a more stringent assumption was used that the deep subsurface water had no bomb radiocarbon).The source for bomb radiocarbon in the surface layer is the carbon dioxide gas exchange with the atmosphere. With this rate taken as 16 mol m^{-2} year^{-1} in *Broecker and Peng* [1982] and as 22 mol m^{-2} year^{-1} in *Broecker et al.* [1978], they find an upwelling of 17×10^6 m^3 s^{-1}. Recent measurements presented in *Smethie et al.* [1985], *Andrié et al.* [1986], and *Oudot et al.* [1987] show a large variability in measured piston velocities and computed gas exchange rates across the equatorial Atlantic, suggesting that the upwelling rate is not tightly determined by this method.

Broecker et al. [1978] also comment that upwelling should induce a fast decrease of surface tritium concentration (8% per year). However, lower decrease values are observed, which suggest [*Broecker and Peng*, 1982] that there is some renewal of the equatorial waters from the northern hemisphere reservoir; therefore a relaxation of the one-dimensional assumption is required. Accordingly, this should push upwelling estimations toward larger values than *Broecker et al.* [1978], because off-equatorial waters also contain large values of bomb radiocarbon. However, analysis could be more complicated, due to the time elapsed for the waters to reach the equator.

Our estimate of the average upwelling rate is smaller than these estimates. Although we are not compelled to correct our approach in order to fit these estimates, our approach also has flaws which could explain a larger transport. For example, if we had imposed a higher heat input into the surface layer to include the heat transport by instability

waves [*Weisberg and Weingartner*, 1988], we would probably have retained solutions corresponding to larger transports into the surface layer (at least for the western box).

7. CONCLUSION

Entrainment of thermocline water in the surface layer when the equatorial thermocline upwells is the main reason for surface layer seasonal cooling. Most of the waters entrained into the surface originate from isopycnals close to the base of the surface layer. A colder temperature is reached in the eastern equatorial Atlantic because the thermocline uplift is stronger and brings colder thermocline water close to the surface. During the upwelling season, there is also increased mixing in the thermocline penetrating down to the equatorial undercurrent core. This mixing explains the seasonal erosion of the EUC maximum salinity, because surface waters above the EUC are often fresher. Mixing probably also decelerates the undercurrent upper part so during the upwelling season the velocity core is found at a larger density in the eastern equatorial Atlantic. Early in the year and particularly in early 1984, there is little mixing in the upper thermocline. The salinity tongue associated with the Equatorial Undercurrent extends eastward in the Gulf of Guinea, as proposed in *Piton and Wacongne* [1985].

The turbulent heat fluxes found here are a little higher than published estimates (diffusion coefficient of the order of 2×10^{-4} m^2 s^{-1}), although still in a feasible range, as is the net seasonally averaged influx into the mixed layer (11×10^6 m^3 s^{-1}). Even so, the diapycnal mass fluxes across surfaces below $\sigma_\theta = 25.0$ are not large compared to the vertical seasonal displacement (even at $\sigma_\theta = 25.0$, they correspond to a vertical uplift of 25 m in a year, scaling it over 3° of latitude). This justifies the use of deep isotherms to illustrate upper layer horizontal mass redistribution, as was done for the climatology in *Merle* [1983], *Hastenrath and Merle* [1987], and for 1983–1984 in *Houghton and Colin* [1986] and *Reverdin et al.* [1991]. The subsurface fluxes and, in particular, their vertical profiles are subject to question because the analysis is hampered by high uncertainties caused by approximations and by limited sampling of variability by the eight cruises.

To put these fluxes into broader perspective, our solution is illustrated in Figure 18. As discussed in *Metcalf and Stalcup* [1967], there is no direct connection along the coast of Brazil between the southern and northern gyres thermocline waters. They argue, the Equatorial Undercurrent results from mixing of source water from the south Atlantic with recycled older water with low-salinity found off the equator. We apply this idea to the 35°W section, assuming that there is no vertical mixing in these water masses further west. We estimate that 9.4×10^6 m^3 s^{-1} of the EUC transport above 15°C originate from the south Atlantic, the remaining 8.6×10^6 m^3 s^{-1} originating from off-equatorial pockets of low-salinity water. During the eastward equatorial route, and along the coasts of equatorial Africa, a volume of 11×10^6 m^3 s^{-1} is entrained in the surface layer. The remainder, transformed into low-salinity water, isopycnally leaves the EUC. Because low-salinity water flow in the east roughly matches the inflow of water with comparable salinity into the undercurrent, we conclude the low-salinity water pockets are mainly formed of recirculated water from the EUC. In this balance, there is no export of upper thermocline waters

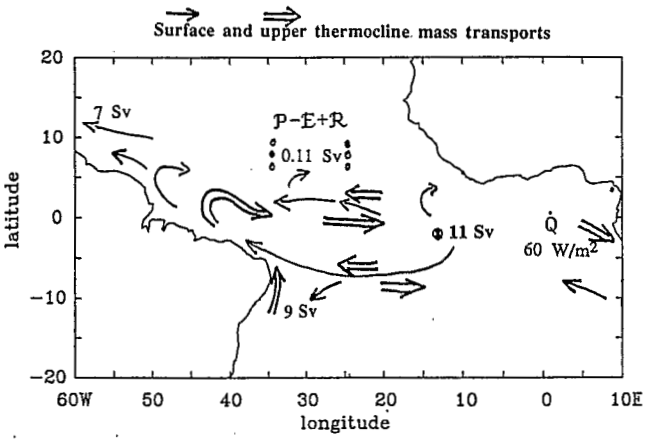

Fig. 18. Sketch of equatorial circulation for surface layer (thin arrow and numbers) and upper thermocline (thick arrows and numbers). Net upwelling, heat (Q), and fresh water ($\mathcal{P} - \mathcal{E} + \mathcal{R}$) budgets are also summarized.

toward the Caribbean, unless some of the upwelled water is reentrained in the thermocline. This absence of a thermocline northward flow is quite coherent with observations off northern South America as first described by *Metcalf and Stalcup* [1967].

The surface layer flux ($T > 24$°C) of equatorial origin entering the Caribbean has been estimated to be 7.1×10^6 m^3 s^{-1} by *Schmitz and Richardson* [1991]. This number is comparable to the results of the inversion by *Roemmich* [1983]. This therefore is the upwelled water main route. There is little evidence for a large near-surface flow into the southern gyre [*Molinari*, 1983; *Reverdin and McPhaden*, 1986], and it is not clear what happens to the remaining surface flow.

With this highly simplified circulation, we can also assess annually and spatially averaged heat and fresh water flux in the equatorial band (range 8°N–8°S). We will neglect turbulent fluxes across 26.4 (based on small turbulent fluxes found at 26.5), and consider the heat and salt budget of the water above it. The surface water flow originating from the equatorial band and penetrating into the Caribbean has an average $T = 27$°C, the average temperature of the southern origin source waters in the EUC is $T = 21.7$°C. If there is no diapycnal flux across 26.4, this implies an average heat gain of 0.20×10^{15} W (assuming 9×10^6 m^3 s^{-1} of water been converted). This is strikingly less than the 0.87×10^{15} W estimated by *Roemmich* [1983]. Of course, even small diapycnal fluxes across the lowest interface could change our heat balance (2×10^6 m^3 s^{-1} across 26.4 would imply an extra 0.10×10^{15} W). We assume a salinity of 36.0 psu for the outflow (slightly more than the surface inflow into the Caribbean, but the salinity of the other outflowing water is unknown), as the incoming waters have an average salinity of 36.39 psu, there is a net fresh water input of 0.11×10^6 m^3 s^{-1}, within the range of the direct estimates of *Baumgartner and Reichel* [1975] and *Yoo and Carton* [1990].

Although this large-scale view is quite realistic, we should not forget that limitations of this study are significant, particularly because of insufficient sampling: barely resolving the seasonal cycle which strongly modulates diapycnal processes at the equator. Because of these uncertainties, we are unable to ascribe certain inconsistencies to incorrect assumptions on the dynamics of the near-equatorial circula-

tion. There was therefore more latitude to adjust solutions than we hoped. Notice in particular that the diapycnal velocities are constrained to some extent by external considerations on the surface layer heat budget, and that no satisfying near-equatorial surface layer salt budget could be obtained.

APPENDIX A: DIAPYCNAL VELOCITY AND EVOLUTION ALONG ISOPYCNAL SURFACES

The approach is parallel to *McDougall*'s [1984], but additional approximations are made as follows.

1. Horizontal (isopycnal) mixing is neglected (induced cabelling small compared to equatorial vertical velocities).

2. $\{\overline{\omega'\theta'}, \overline{\omega'S'}\} = -K\{\theta_z, S_z\}$, i.e., an eddy coefficient formulation for vertical eddy transports, in which we neglect double diffusive effects.

3. Instead of neutral surfaces, σ_θ surfaces are used (small differences with the more correct isopycnal surfaces for depths shallower than 150 m).

The equations for the isopycnal evolution of salinity and temperature are

$$\left(\frac{\partial\theta}{\partial t}\right)_{\sigma_\theta} + U\nabla_{\sigma_\theta}\theta + \omega\frac{\partial\theta}{\partial z} = \frac{\partial\,(K\,\partial\theta/\partial z)}{\partial z} + \frac{\dot{Q}_z}{\rho\, c_p} \qquad \text{(A1)}$$

$$\left(\frac{\partial S}{\partial t}\right)_{\sigma_\theta} + U\nabla_{\sigma_\theta}S + \omega\frac{\partial S}{\partial z} = \frac{\partial\,(K\,\partial S/\partial z)}{\partial z} \qquad \text{(A2)}$$

with usual notations; Q refers to the radiative fluxes, ω to diapycnal velocity, and c_p the heat capacity.

Multiplying (A1) by ρ_θ and (A2) by ρ_S, where $\rho_\theta = \partial\rho/\partial\theta_{|S}$, $\rho_S = \partial\rho/\partial S_{|\theta}$, and ρ is potential density, results in

$$\omega\frac{\partial\rho}{\partial z} = \rho_\theta\frac{\partial\,(K\,\partial\theta/\partial z)}{\partial z} + \rho_S\frac{\partial\,(K\,\partial S/\partial z)}{\partial z} + \rho_\theta\frac{\dot{Q}_z}{\rho\, c_p} \qquad \text{(A3)}$$

because $\rho_\theta\nabla_{\sigma_\theta}\theta + \rho_S\nabla_{\sigma_\theta}S = 0$ and $\rho_\theta\,\partial\theta/\partial t + \rho_S\,\partial S/\partial t = 0$. This can be rewritten as

$$\omega = K_z + \frac{\rho_\theta\theta_{zz} + \rho_S S_{zz}}{\rho_z}K + \rho_\theta\frac{\dot{Q}_z}{\rho c_p \rho_z}$$

Replacing ω by this expression in (A2) results in

$$\left(\frac{\partial S}{\partial t}\right)_{\sigma_\theta} + U\nabla_{\sigma_\theta}S = -K\frac{\rho_\theta}{\rho_z}S_z^2\left(\frac{\theta_z}{S_z}\right)_z - \rho_\theta\frac{S_z\dot{Q}_z}{\rho_z c_p}$$

The first term on the right-hand side combines both the effect of mixing and diapycnal advection, which is a consequence of the Fickian approximation for small-scale turbulence. For diagnostic studies, it has the nice property of being proportional to K and not involving its derivative. A similar equation (and equivalent) is easily derived for temperature. For a more complete derivation, including transports by horizontal eddies, the reader is referred to *McDougall* [1984].

APPENDIX B: SALINITY

B1. Accuracy of the Conductivity Probe

During the FOCAL cruises on the R.V. *Capricorne*, salinity estimated from measurements of a Neil-Brown CTD probe differed systematically from other data collected in 1983–1984. We will show that salinity is underestimated by the FOCAL data at 35°W, 23°W, and 4°W, and that a correction can be implemented.

Water masses between 100–200 m and 600–700 m originate mainly from the South Atlantic [*Sverdrup et al.*, 1942] with a boundary of the central North Atlantic water located near 1°N. In the equatorial area east of 30°W, the central waters have a well-defined T–S curve, which is almost linear and exhibits little zonal variability in the temperature range from 14°C to 7°C. We do not expect large variations of this water characteristic within the 2-year program, but to verify we will compare other cruises (TTO–TAS, AJAX leg 1, a cruise by the R.V. *Lynch*, and a cruise by the R.V. *Wylkes* (referred to as set 4)).

The comparison of the FOCAL cruises and these other cruises is carried between 5°N and 5°S. For each pair of close profiles, salinities at eight temperatures (between 7°C and 14°C) are compared when available (every degree in latitude, except for set 4, for which fewer stations are available). To summarize the comparison, all pairs are combined for a given cruise, and shown in Table B1. Usually, these comparisons include pair of stations at the same latitude and longitude. For TTO and the R.V. *Lynch* cruise at 28°W, where no FOCAL station was available at this longitude, a linear interpolation is carried between the FOCAL sections at 23°W and 35°W. The time difference between the pair of stations compared is usually less than a month, except for AJAX, which took place 40 days before a FOCAL cruise. The comparison presented in Table B1 clearly shows that after the January 1983 FOCAL 2 cruise, a large shift of the estimated salinity between 0.030 and 0.060 occurred. For a given cruise, the standard deviation between the different points of comparison is much less, between 0.011 and 0.020. This suggests that the differences are systematic and a correction can be sought. Unfortunately, no cruise was available for the validation of FOCAL cruises 0, 1, 3, 6.

The conductivity probe was calibrated at the start of the program, but not during the next 4 years. In order to determine if water masses remained steady during the 2-year span of the field experiment, we will select a reference cruise (FOCAL 0 or FOCAL 1), and investigate whether the evolution follows the one indicated by Table B1 (the stations retained are along 23°W and 4°W: we exclude 35°W, where more variability is observed).

Choosing FOCAL 0, we find that the shift of the probe is not linear in time (FOCAL 7 is a maximum, but FOCAL 6

TABLE B1. Comparison of the Salinity of the FOCAL Cruise and Other Nearly Simultaneous Cruises (Isotherms Between 14°C and 7°C)

Cruise	Number of Stations	Average Lag, Days	Average Difference, psu	rms Difference, psu
FOCAL2–TTO 28°W, Jan. 1983	7	20	−0.002	0.020
FOCAL4–Lynch 28°W, July 1983	6	5	−0.030	0.016
FOCAL5–AJAX 4°W, Oct.–Nov. 1983	9	40	−0.060	0.016
FOCAL7–Wylkes 4°W, May–June 1984	8	40	−0.056	0.011

TABLE B2. Correction Applied to the Salinity for Each of the R.V. *Capricorne* FOCAL Cruises

	FOCAL Cruise								
	0	1	2	3	4	5	6	7	8
ΔS, psu	0.014	0.014	0.010	0.046	0.044	0.056	0.048	0.062	0.062
rms, psu		0.016	0.010	0.014	0.011	0.014	0.013	0.012	0.017

The rms deviations correspond to the comparison to cruise FOCAL0.

is not very shifted). The differences along 23°W and along 4°W usually compare well, with the exception of FOCAL 6 and especially FOCAL 1. This suggests to us that the probe drifted during FOCAL1 (maybe between the 23°W cruise and the 4°W), probably by up to 0.02. The evolution in time follows what could be assessed from the comparison with the other cruises (Table B1), and this suggests that the water masses have remained remarkably stable. We will therefore adopt the assumption that salinity does not evolve in this range, and correct from the comparison of FOCAL 0. Indeed, the other cruise data are also very close to the GATE data in 1974.

However, from the other cruise data, we find that FOCAL 0 shifted by about 0.014, and this is included in the correction presented in Table B2. The assumption is also made that the same correction can be applied to the whole temperature and depth range sampled by the probe.

B 2. Sampling Error

Investigation of the diapycnal processes is based on how salinity evolves as it advects downstream with the equatorial undercurrent. It is therefore particularly important to estimate our ability to reconstruct seasonal time series of salinity from cruise data. During the upwelling season, the T–S relationships indicate an eastward decrease (Figure 3, and earlier in *Katz et al.* [1979]). The seasonal dependence of this effect is large as reported earlier (*Voituriez* [1981] or *Hisard and Hénin* [1987] for the FOCAL cruises). Therefore the question is to evaluate how well the variability is captured. This is illustrated (Figure B1*a*) for the 25.5 surface at 4°W, where three other meridional cruises are available with a meridional sampling not as good (0.66° or even 0.75° degree of latitude) as for FOCAL. The three other cruises fit with some scatter to the curve. This may imply errors in timing by a month or two but does not suggest a large missing peak or trough. Shallower up (24.50), the stations did not show the presence of salinity greater than 36.50 psu, which have certainly flowed across 4°W on their way to 6°E (sampled in May 1984 [*Piton and Wacongne*, 1985]). These large values are not present in the interpolated time series but errors on the order of 0.1 remain in the uncertainty range of these curves.

In the surface layer near the equator, uncertainty is much larger (errors on the order of 0.2 psu), because high-frequency displacements of the near-equatorial salinity front induce a variability which is comparable to the low-frequency changes (Figure B1*b*, where reference is based on salinity data from a ship-of-opportunity program, A. Dessier, personal communication, 1990).

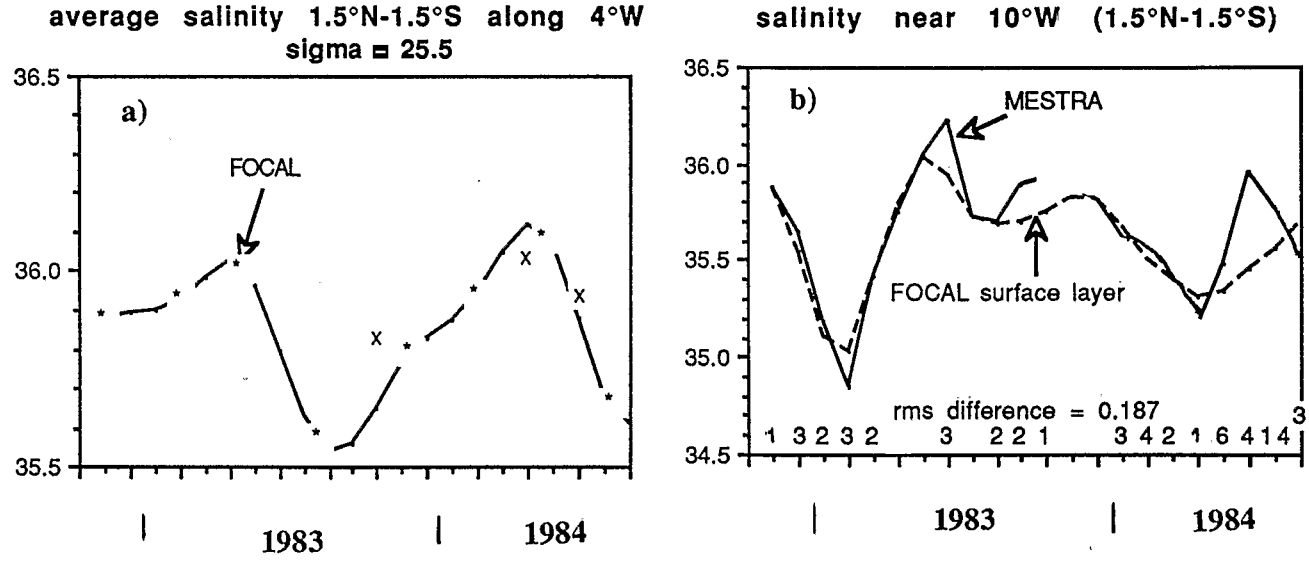

Fig. B1. Comparison between salinity time series reconstructed from the FOCAL cruises and other data (we present only the 1.5°N–1.5°S meridional averages). (*a*) Subsurface salinity on $\sigma_\theta = 25.5$. The stars correspond to the FOCAL cruises, and the crosses to the three other available cruises in the vicinity of 4°W. (*b*) Comparison of the FOCAL surface layer (vertical average of the layer with temperature within 1° of the sea surface) with the MESTRA file (communication of A. Dessier, 1990) composed primarily of ship-of-opportunity samples (the monthly number of profiles is indicated above the lower axis).

APPENDIX C: ZONAL CURRENTS

C 1. Accuracy of the Current Profiles

During the FOCAL cruises of the R.V. *Capricorne*, the current profile from 0 to 500 m was collected with a profiler. This profiler includes an Aanderaa RCM4 current meter falling freely along a cable attached under a drifting buoy (an earlier prototype is presented in *Düing and Johnson* [1976]). Current profiles were also collected at 1°E and 6°E from the R.V. *Nizery*, where the cable was attached to the ship.

To validate current profiles from the R.V. *Capricorne*, we compare them with simultaneous current data (VACM) from three equatorial moorings at 28°W, 24°W, and 4°W [*Weisberg et al.*, 1987]. The currents from the profiler were interpolated at 5 dbar spacing and further vertically smoothed with a 1,2,1 running mean over adjacent bins. The moored current meter data were hourly averaged. The profile was usually collected in close vicinity of the mooring, except for one instance at 28°W and one at 24°W, where the profile is 1° of longitude apart from the mooring (in this instance, the mooring currents were daily averaged).

The results for the three longitudes are shown in Figure C1. On the average, the current profiler underestimates the current at each depth sampled by the mooring current meters. At each individual mooring site, there are few comparisons (with a maximum of six points), but the average profile of the difference profiler-mooring has similar characteristics at the three longitudes.

The largest difference (about 20 cm/s) is found in the core of the undercurrent: it is also where the standard deviation of the comparisons is minimum. Below 200 m at 28°W, the mean difference diminishes to 2.5 cm/s, and null at 300 m at 24°W in the average. At 10-m depth, the difference is

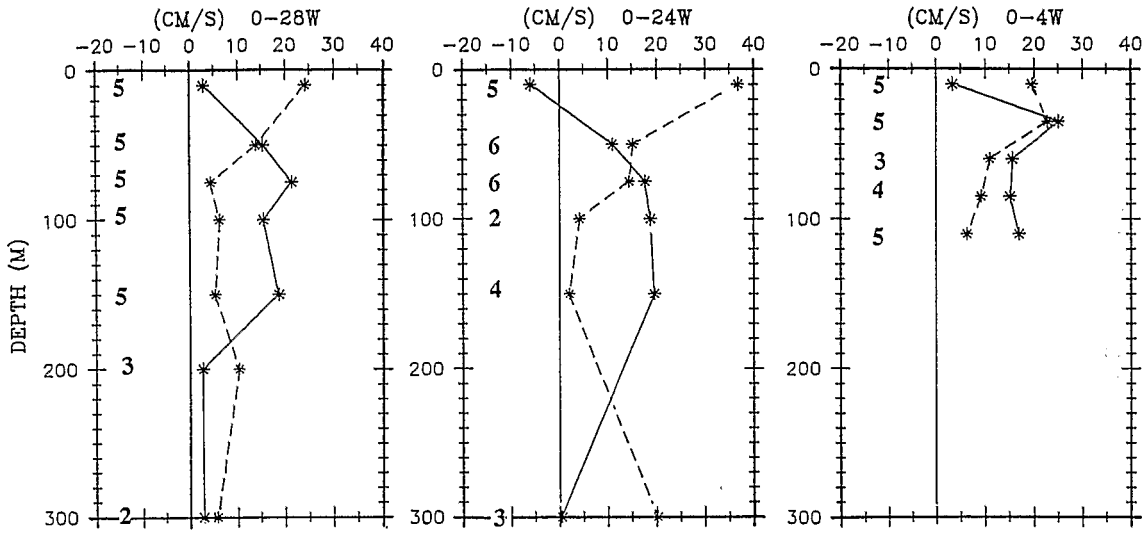

Fig. C1. Comparison between currents estimated from the profiler and simultaneous current meter measurements at nearby moorings. The average profile (solid line) as well as the standard deviation (dashed line) of the difference are shown for the three mooring locations. The number of comparisons is indicated in the left margin at each current meter depth.

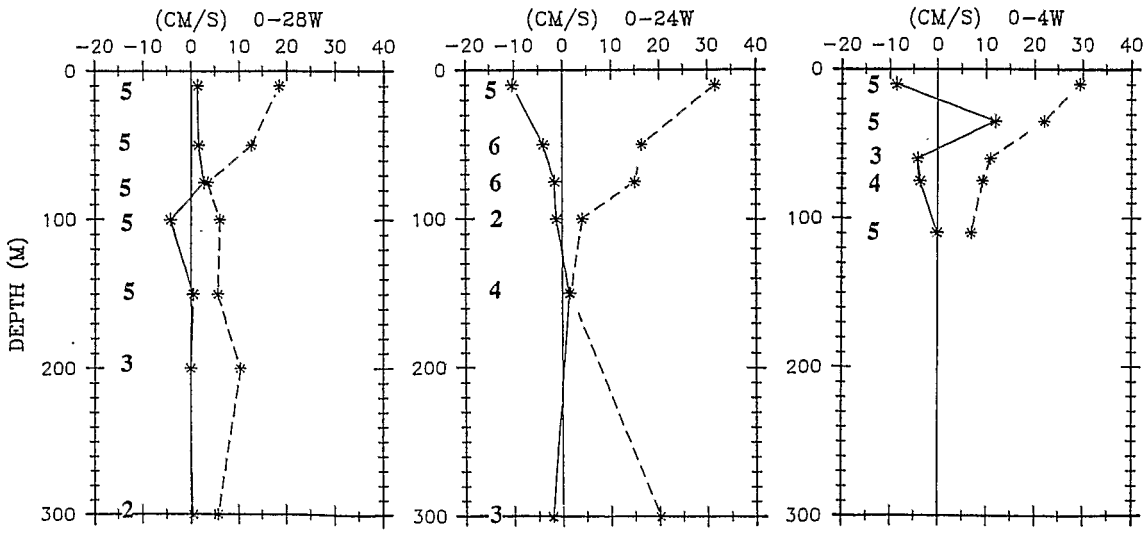

Fig. C2. Same as Figure C1, but after applying the corrections to the profiler data.

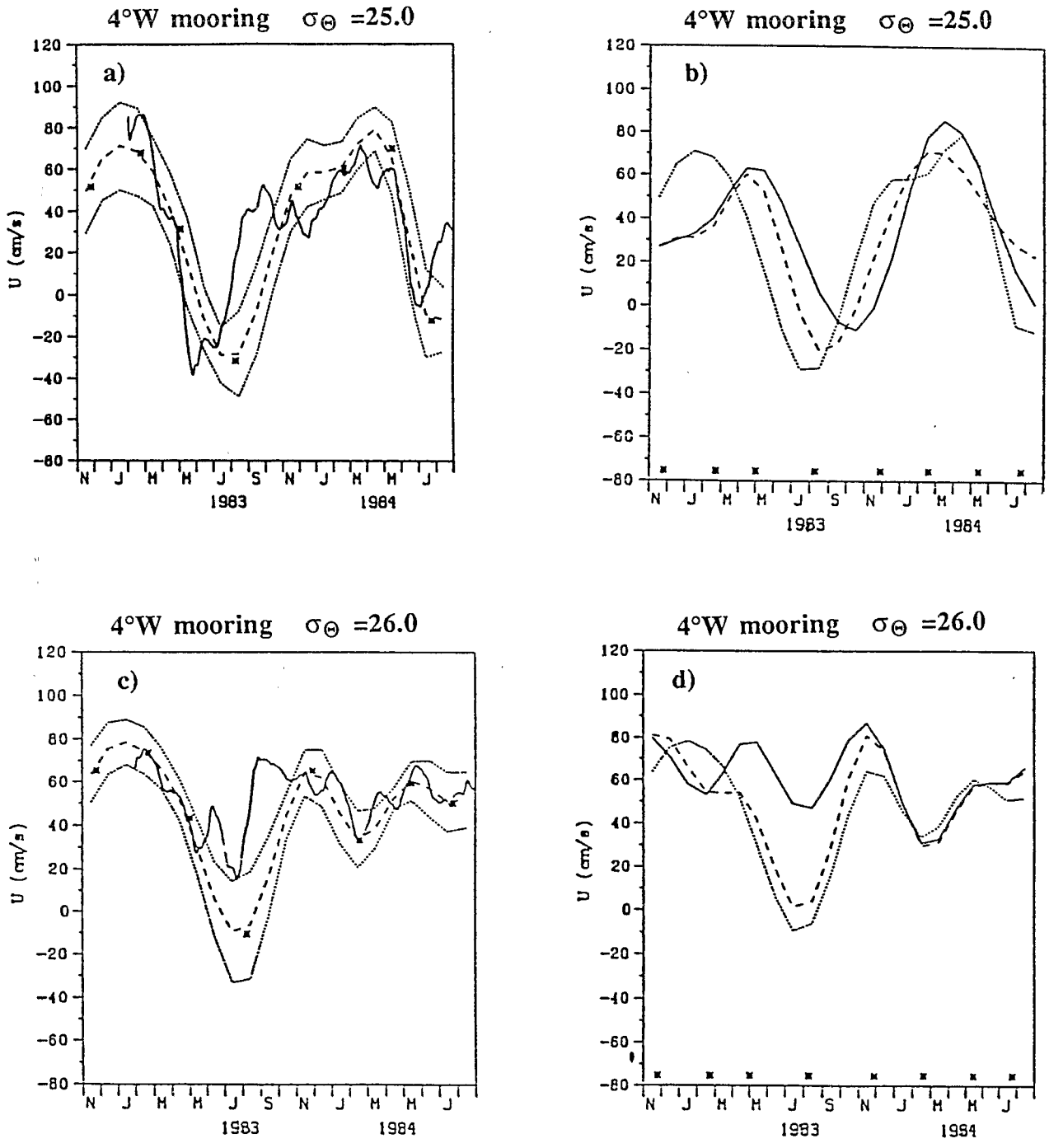

Fig. C3. Analysis on selected ispoycnals of the zonal current from a current meter mooring at (0°, 4°W) and from profiler stations at the same locations. (*a*) Surface $\sigma_\theta = 25.0$, Solid line shows the mooring data interpolated linearly to the level estimated from temperature and a seasonally θ–S relationship (the series have been filtered by a 1-month running mean average). Dashed line shows time series from the profiler reconstituted by a cubic spline from the discrete sampling of the current at the current meter levels (stars). The error range indicated by the two dotted lines was estimated by sampling the mooring time series at 3-month intervals and estimating the dispersion of the cubic spline reconstituted time series. (*b*) Solid line shows the profiler time series from the values of the full profile interpolated at the isopycnal horizon, dashed line shows sampling at the current meter depths as on Figure C3*a*. Dotted line shows sampling of the current meter time series at the time of the FOCAL stations (stars along the lower axis). (*c* and *d*) Same as Figures C3*a* and C3*b*, but for $\sigma_\theta = 26.0$.

less than 5 cm/s, but the standard deviation is large, particularly at 24°W. This suggests that the profiler is not an adequate instrument at this depth, and we estimate that the measurements are reliable only below 15 m.

Similar comparisons made by *Freitag and Firing* [1984], using a Düing type profiler hanging under a vessel and moored current meters at 150°W, also show that the profiler underestimates the velocity at the core of the EUC (by

17 cm/s). In this instance, the current profiler was referenced to the mean current between 300 and 500 m (for FOCAL cruises, referencing currents at these depths does not improve the comparison). It is difficult to state why we observe these systematic differences because we do not know the shape of the cable under intense vertical shear or the tilt of the profiler body. Therefore, the following corrections have been implemented.

1. A barotropic shift of 2.5 cm s^{-1} of the profile applied between 1°N and 1°S to compensate the differences found at 200 and 300 m. With an EUC of a 100-m thickness between 1°N and 1°S, this modifies estimation of the transport by 0.5×10^6 m^3 s^{-1}.

2. An idealized profile of a correction based on the mean profile of the difference. The maximum correction is 15 cm s^{-1} at the level and latitude of the EUC velocity core. We then reduce the correction to 12 cm s^{-1} at a distance of 0.5° and 6 cm/s at a distance of 1°. This assumes that the difference is related to the shear.

3. The current between 0 and 15 m is assigned the value at 15 m. Of course, there is a shear in the upper layer, but we have no satisfactory estimate of it.

After applying these corrections, a final comparison is reported on Figure C2. Some systematic differences remain, in particular, at 150 m, but the large ones in the EUC core have disappeared. The correction was too large in the surface layer, but this difference is not significant because of the larger uncertainty there. The random uncertainty has slightly increased, but on the average remains less than 10 cm/s in the thermocline.

C 2. Sampling Error

Mooring data are available at discrete vertical levels along the equator at 28°W, 24°W, 15°W, and 4°W close to profiler stations. The comparison of our analysis to isopycnal surfaces with the mooring is not straightforward, as vertical interpolation of the mooring records to these surfaces is required. We made the following comparisons.

1. We sample the mooring time series at 3-month intervals to evaluate uncertainty associated with sampling, and compare the mooring time series with the profiler time series constructed assuming the same vertical sampling.

2. We compare the time series constructed from the profiler with the mooring vertical sampling (Figure C3*a*) with respect to the full vertical sampling (Figure C3*b*). We also show the mooring time series sampled at the time of the FOCAL cruises (Figure C3*c*); this curve differs from that in Figure C3*a* only due to the random differences after the correction of the bias.

The results are illustrated at two levels for the 4°W mooring (Figure C3). The $\sigma_\theta = 25.0$ surface is above the core of the EUC. Figure C3*a* shows that the minimum of the current in the 1983 upwelling season would appear 1 month later than really observed if interpolated from the mooring sampled during the FOCAL cruises. In this instance, Figures C3*a* and C3*c* also have a large rms difference (Figure C3*b*). There is also a noticeable difference for the cruise data introduced by the vertical sampling at discrete levels. The effect is even more noticeable at 26.0 (Figures C3*c*, C3*d*), a surface usually below the core of the EUC, where the profiler seems to be quite accurate (the small rms difference between the profiler and the current meters shown in Figure C2 results in the closeness between Figures C3*a* and C3*c*).

For this eastern location (4°W), we therefore find that the vertical distribution of the sensors along the mooring line is insufficient to construct time series on isopycnal surfaces. This effect (not so pronounced at other moorings) and the absence of off-equatorial moorings to resolve the meridional structure of the undercurrent induce us to use the less accurate profiler data for our analysis. Errors associated with the time sampling range between 10 cm/s in the core of the thermocline to 20 cm/s near the surface and are larger than the instrument errors. These errors together are often comparable to seasonal variability, so that, as a pessimistic alternative in our subsurface budgets, we will ignore the time variability of the currents.

APPENDIX D: UNCERTAINTY ON THE DIAPYCNAL VELOCITY

There are two types of errors involved in estimating diapycnal velocity. One is associated with discrete sampling which can alias subseasonal variability (Appendixes B and C). The other is associated with approximations done (the method error). For average velocity, an upper estimate of the sampling error is given by $\text{rms} * n^{-1/2}$, where n is the number of cruises and rms is the standard deviation within the set. This is likely to be an overestimate, because the seasonal variability which contributes to the rms is not associated with an error on the average value. The sampling error for case A is, however, coherent with a more direct estimate of the error on u and v based on the comparison with mooring and sea level time series. This more direct error estimate was used to evaluate seasonal errors on the terms of (7) (Figure 10).

Because we do not a priori know what is the best method to estimate diapycnal velocity, the method error is investigated by comparing approaches based on different approximations, which are hoped to include the correct one. In Figure D1, three estimates based on different estimates of the meridional velocity are shown for the eastern box with the same reference level ($\omega = 0$ at $\sigma_\theta = 26.4$ and at $\sigma_\theta = 27.0$; the last isopycnal is near 400 m). In typical fashion, the sampling errors are large, so that differences between different average estimates of diapycnal velocity are not significant. The average profile uncertainty is large, in particular in the lower part, where the average is not significantly different from 0. The rms variability is smaller in case A and B, than case C. This is rather logical, as C results from meridional integration and uses the more noisy current measurements. This at least suggests that case C seasonal estimates of ω are mostly noise.

The diapycnal velocity profiles are more sensitive to the reference surfaces than to the method used in estimating v. For example, if instead of selecting $\sigma_\theta = 26.8$ and $\sigma_\theta = 27.0$ as the two levels where ω is 0, we chose $\sigma_\theta = 26.9$ and $\sigma_\theta = 27.0$, the average transport into the mixed layer approximately increases by 20%, and the diapycnal transport across $\sigma_\theta = 25.0$ would increase by 30% (Table 1). Error on the zonal convergence were not estimated. Because an important share of the diapycnal vertical velocity is related to the zonal convergence obvious in Figure 6, this could also have a large effect on ω.

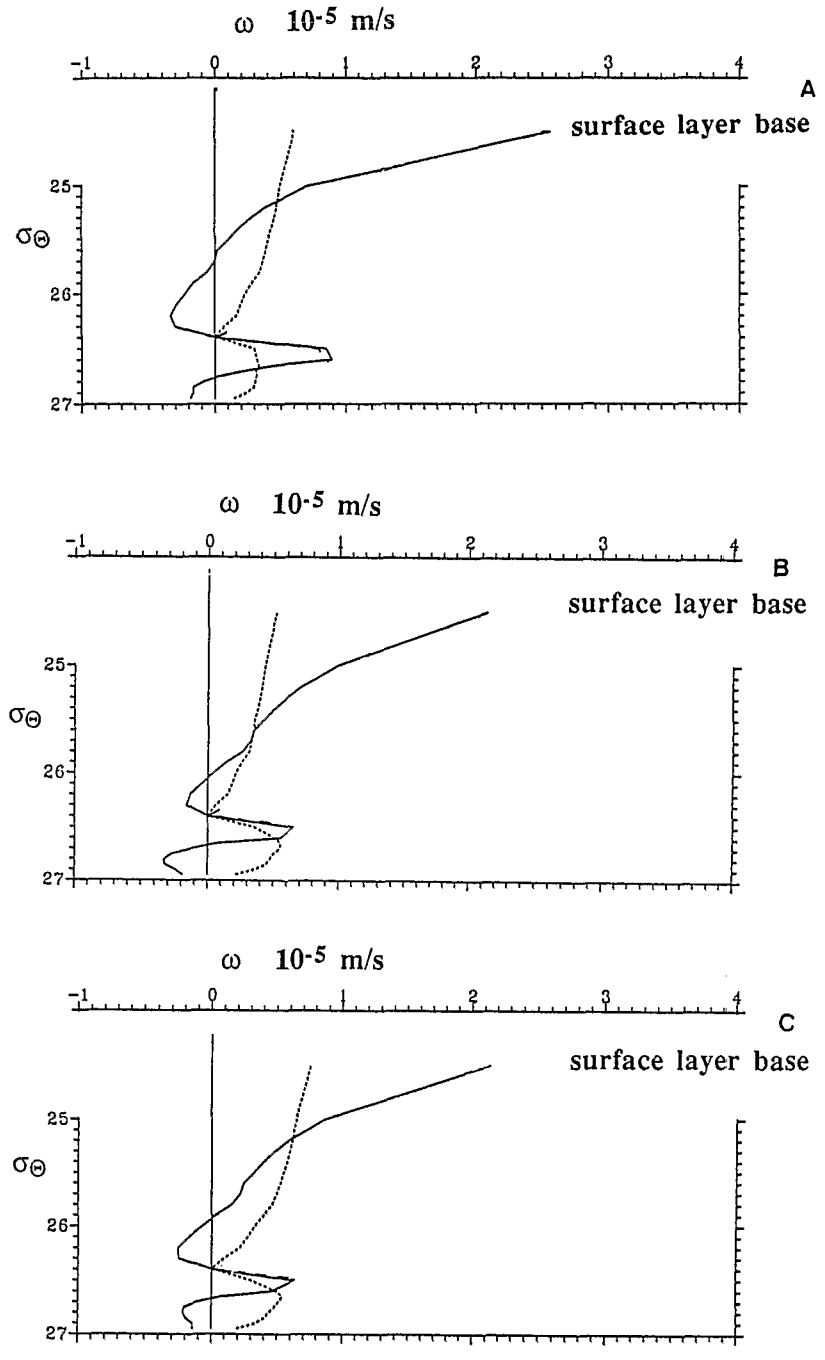

Fig. D1. Diapycnal velocity (solid line) scaled over a 1° meridional band estimated by the three methods for the eastern box. In each case, we also impose $\omega = 0$ at $\sigma_\theta = 26.4$ and $\sigma_\theta = 27.0$. The entrainment velocity into the mixed layer is also shown (the mass budgets have been balanced to a zero vertical velocity at the sea surface by applying a correction in the surface layer). Dotted line shows rms uncertainty.

Acknowledgments. The elements for this paper are contained to a large extent in the Thèse de Doctorat of Yves Gouriou, defended at the Pierre et Marie Curie University in Paris on December 10, 1990. We are strongly indebted toward our colleagues of ORSTOM, who performed with dedication the FOCAL cruises in 1982–1984, and bore with patience our questions on the data calibration. This project was supported by the French Programme national pour l'étude de la dynamique du climat. Discussions with Sophie Wacongne provided another insight on the same scientific problem. Comments on the manuscript by Mark Cane and Eli Katz as well as by the two reviewers were helpful. Support for one author, G.R., was obtained through generous gifts from the G. Lenger Vetlesen Fundation, members of IPIECA, and a grant jointly funded by the National Science Foundation and NOAA, OCE90-00127.

REFERENCES

Andrié, C., C. Oudot, C. Genthon, and L. Merlivat, CO_2 fluxes in the tropical Atlantic during 1983–1984, *J. Geophys. Res.*, *91*, 11,741–11,755, 1986.

Baumgartner, A., and E. Reichel, *The World Water Balance: Mean Annual Global, Continental and Maritime Precipitation, Evaporation and Run-off*, 179 pp., 31 pp. maps, Elsevier, New York, 1975.

Brady, E. C., and H. L. Bryden, Estimating vertical velocity on the equator, *Oceanol. Acta, Spec. Vol.*, *6*, 33–38, 1987.

Broecker, W. S., and T. H. Peng, *Tracers in the Sea*, 690 pp., Eldigio Press, Lamont-Doherty Geological Observatory of Columbia University, Palisades, New York, 1982.

Broecker, W. S., T. H. Peng, and M. Stuiver, An estimate of the upwelling rate in the equatorial Atlantic based on the distribution of bomb radiocarbon, *J. Geophys. Res.*, *83*, 6179–6186, 1978.

Bryden, H. L., and E. C. Brady, Diagnostic model of the three dimensional circulation in the upper equatorial Pacific Ocean, *J. Phys. Oceanogr.*, *15*, 1255–1273, 1985.

Bryden, H. L., and E. C. Brady, Eddy momentum and heat fluxes and their effects on the circulation of the equatorial Pacific Ocean, *J. Mar. Res.*, *47*, 55–79, 1989.

Crawford, W. R., and T. R. Osborn, Microstructure measurements in the Atlantic equatorial undercurrent during GATE, *Deep Sea Res.*, *26*, *GATE Suppl. II*, 285–308, 1979*a*.

Crawford, W. R., and T. R. Osborn, Energetics of the Atlantic equatorial undercurrent, *Deep Sea Res.*, *GATE Suppl. II*, *26*, 309–324, 1979*b*.

Dillon, T. M., J. N. Moum, T. K. Chereskin, and D. R. Caldwell, Zonal momentum balance at the equator, *J. Phys. Oceanogr.*, *19*, 561–570, 1989.

Düing, W., and D. Johnson, High resolution current profiling in the strait of Florida, *Deep Sea Res.*, *19*, 259–274, 1972.

Düing, W., P. Hisard, E. Katz, J.Meincke, L. Miller, K. Moroshkin, G. Philander, A. Ribnikov, K. Voigt, and R. Weisberg, Meanders and long waves in the equatorial Altantic, *Nature*, *257*, 280–284, 1975.

Esbensen, S. K., and Y. Kushnir, The heat budget of the Global Ocean: an Atlas based on estimates from marine surface observations, Climatic Res. Institution, *Rep. 29*, Oregon State Univ., Corvallis, 27 pp., 188 fig, 1981.

Fahrbach, E., J. Meincke, and A. Sy, Observations of the horizontal separation of the salinity core and the current core in the Atlantic equatorial Undercurrent, *J. Mar. Res.*, *44*, 763–779, 1986.

Freitag, H. P., and E. Firing, Comparison of profiling and moored current measurements in the equatorial Pacific, *J. Phys. Oceanogr.*, *89*, 3724–3728, 1984.

Garçon, V., L. Martinon, C. Andrié, P. Andrich, and J. F. Minster, Kinematics of CO_2 fluxes in the tropical Atlantic Ocean during the 1983 northern summer, *J. Geophys. Res.*, *94*, 855–870, 1989.

Halpern, D. R., A. Knox, D. S. Luther, and S. G. H. Philander, Estimates of equatorial upwelling between 140° and 110°W during 1984, *J. Geophys. Res.*, *94*, 8018–8020, 1989.

Hastenrath, S., and P. Lamb, *Heat Budget Atlas of the Tropical Atlantic and Eastern Pacific Oceans*, 90 pp., University of Wisconsin Press, Madison, 1978.

Hastenrath, S., and J. Merle, Annual cycle of subsurface thermal structure in the tropical Atlantic Ocean, *J. Phys. Oceanogr.*, *17*, 1518–1538, 1987.

Hénin, C., P. Hisard, and B. Piton, Observations hydrologiques dans l'océan Atlantique équatorial (juillet 1982–août 1984), *Trav. Doc. ORSTOM, sér. FOCAL*, *196*, 191 pp, 1987.

Hisard, P., and C. Hénin, Response of the equatorial Atlantic ocean to the 1983–1984 wind from the Programme Français Océan et Climat dans l'Atlantique équatorial cruise data set, *J. Geophys. Res.*, *92*, 3759–3768, 1987.

Houghton, R., Influence of local wind forcing in the Gulf of Guinea, *J. Geophys. Res.*, *94*, 4816–4828, 1989.

Houghton, R. W., and C. Colin, Thermal structure along 4°W in the Gulf of Guinea during 1983–1984, *J. Geophys. Res.*, *91*, 11,727–11,739, 1986.

Houghton, R. W., and C. Colin, Wind-driven meridional eddy heat flux in the Gulf of Guinea, *J. Geophys. Res.*, *92*, 10,777–10,786, 1987.

Hsiung, J., Mean surface energy fluxes over the global ocean, *J. Geophys. Res.*, *91*, 10,585–10,606, 1986.

Katz, E. J., J. G. Bruce, and D. P. Petrie, Salt and mass flux in the Atlantic equatorial undercurrent, *Deep Sea Res.*, *GATE suppl. II*, *26*, 137–160, 1979.

Katz, E. J., R. L. Molinari, D. E. Cartwright, P. Hisard, H. U. Lass, and A. deMesquita, The seasonal transport of the equatorial undercurrent in the western Atlantic (during the Global Weather Experiment), *Oceanol. Acta*, *4*, 445–450, 1981.

Legeckis, R., and G. Reverdin, Long waves in the equatorial Atlantic Ocean during 1983, *J. Geophys. Res.*, *92*, 2835–2842, 1987.

Liu, T., K. Katsaros, and J. Businger, Bulk parameterization of air-sea exchanges of heat and water vapor, including the molecular constraints at the interface, *J. Atmos. Sci.*, *36*, 1722–1735, 1979.

McDougall, T. J., The relative roles of diapycnal and isopycnal mixing in subsurface water mass conversion, *J. Phys. Oceanogr.*, *14*, 1577–1589, 1984.

Merle, J., Atlas hydrologique saisonnier de l'océan Atlantique intertropical, *Trav. Doc. ORSTOM*, *82*, 64 pp, 1978.

Merle, J., Seasonal heat budget in the equatorial Altantic Ocean, *J. Phys. Oceanogr.*, *10*, 464–469, 1980.

Merle, J., Seasonal variability of subsurface thermal structure in the tropical Atlantic Ocean, in *Hydrodynamics of the Equatorial Ocean*, edited by J. C. Nihoul, pp. 31–49, Elsevier, New York, 1983.

Merle, J., M. Fieux, and P. Hisard, Annual signal and interannual anomalies of sea surface temperature in the eastern equatorial Atlantic, *Deep Sea Res.*, *26*, *GATE Suppl. II*, 77–101, 1979.

Metcalf, W. G., and M. C. Stalcup, Origin of the Atlantic equatorial undercurrent, *J. Geophys. Res.*, *72*, 4952–4975, 1967.

Molinari, R. L., Observations of near-surface currents and temperature in the central and western tropical Atlantic Ocean, *J. Geophys. Res.*, *88*, 4433–4438, 1983.

Morel, A., Optical modeling of the upper ocean in relation to its biogenous matter content (case I waters), *J. Geophys. Res.*, *93*, 10,749–10,768, 1988.

Moum, J. N., D. R. Caldwell, and C. A. Paulson, Mixing in the equatorial surface layer and thermocline, *J. Geophys. Res.*, *94*, 2005–2021, 1989.

Neumann, G., Precipitation, evaporation and monthly salinity variations in the inner Gulf of Guinea near the equator, in *Studies in Physical Oceanography*, vol. 1, edited by A. L. Gordon, pp. 19–48, Gordon and Breach, NewYork, 1972.

Neumann, G., W. H. Beatty, and E. Escowitz, Seasonal changes of oceanographic and marine-climatological conditions in the equatorial Atlantic, Final report of the Office of Naval Research, contract NR083-307, 1975.

Niiler, P. P., and J. Stevenson, The heat budget of tropical ocean warm-water pools, *J. Mar. Res.*, *40*, 465–480, 1982.

Osborn, T. R., Estimates of the local rate of vertical diffusion from dissipation measurements, *J. Phys. Oceanogr.*, *10*, 83–89, 1980.

Oudot, C., Observations physico-chimiques et biomasse végétale dans l'océan Atlantique équatorial, Programme PIRAL (juillet 1982–août 1984), *Trav. Doc. ORSTOM, sér. FOCAL*, *209*, 215 pp., 1988.

Oudot, C., C. Andrié, and Y. Montel, Evolution du CO_2 océanique et atmosphérique sur la période 1982–1984 dans l'Atlantique tropical, *Deep Sea Res.*, *34*, 1107–1137, 1987.

du Penhoat, Y., and Y. Gouriou, Hindcasts of equatorial sea surface dynamic height in the Atlantic in 1982–1984, *J. Geophys. Res.*, *92*, 729–3740, 1987.

Peters, H., M. C. Gregg, and J. M. Toole, On the parameterization of equatorial turbulence, *J. Geophys. Res.*, *93*, 1199–1218, 1988.

Peters, H., M. C. Gregg, and J. M. Toole, Meridional variability of turbulence through the equatorial undercurrent, *J. Geophys. Res.*, *94*, 18,003–18,009, 1989.

Picaut, J., Propagation of the seasonal upwelling in the eastern tropical Atlantic, *J. Phys. Oceanogr.*, *13*, 18–37, 1983.

Piton, B., and S. Wacongne, Unusual amounts of very saline subsurface water in the eastern Gulf of Guinea in May 1984, *Trop. Ocean. Atmos. Newslett.*, vol. 32, pp. 5–8, AOML/NOAA, Univ. of Wash., Seattle, 1985.

Reverdin, G., Heat budget of the tropical Atlantic Ocean — Seasonal upwellings, *Deep Sea Res.*, *32*, 363–368, 1984.

Reverdin, G., and M. McPhaden, Near-surface current and temperature variability observed in the equatorial Atlantic from drifting buoys, *J. Geophys. Res.*, *91*, 6569–6581, 1986.

Reverdin, G., and Y. du Penhoat, Modeled surface dynamic height in 1964–1984: An effort to assess how well the low fre-

quencies in the equatorial Atlantic were sampled in 1982–1984, *J. Geophys. Res.*, *92*, 1899–1913, 1987.

Reverdin, G., P. Rual, Y. du Penhoat, and Y. Gouriou, Vertical structure of the seasonal cycle in the central equatorial Atlantic ocean: XBT sections from 1980–1988, *J. Phys. Oceanogr.*, *21*, 277–291, 1991.

Roemmich, D., The balance of geostrophic and Ekman transports in the tropical Atlantic ocean, *J. Phys. Oceanogr.*, *13*, 1534–1539, 1983.

Schmitz, W. J., Jr., and P. L. Richardson, On the sources of the Florida Current, *Deep Sea Res.*, *38*, Suppl. 1, S379–S409, 1991.

Smethie, W. M., T. Takashi, D. W. Chipman, and J. R. Ledwell, Gas exchange and CO_2 flux in the tropical Atlantic Ocean determined from ^{222}Rn and pCO_2 measurements, *J. Geophys. Res.*, *90*, 7005–7020, 1985.

Steger, J. M., and J. A. Carton, Long waves and eddies in the tropical Atlantic Ocean: 1984–1990, *J. Geophys. Res.*, *96*, 15,161–15,171, 1991.

Sverdrup, H. U., M. W. Johnson, and R. H. Fleming, *The Ocean*, 1087 pp., Prentice Hall, Englewood Cliffs, N. J., 1942.

Verstraete, J. M., and J. M. Vassie, The vertical structure of the zonal and meridional pressure gradients in the equatorial Atlantic during 1983 and 1984, *Deep Sea Res.*, *37*, 1–26, 1990.

Voituriez, B., The equatorial upwelling in the eastern Atlantic ocean, Recent progress in equatorial oceanography: A report of the final meeting of SCOR working group 47 in Venice, Italy, April 27–30, 1981, edited by J. P. McCreary, D. W. Moore, and J. M. Witte, pp. 229–247, JIMAR, University of Hawaii, Nova University/N.Y.I.T. Press, 1981.

Voituriez, B., Les variations saisonnières des courants équatoriaux a 4°W et l'upwelling équatorial du Golfe de Guinée, 1, Le sous-courant équatorial, 2, Le courant équatorial sud, *Océanographie tropicale*, *18*, 163–185, 185–1[illegible], 1983.

Wacongne, S., Dynamics of the equatorial undercurrent and its termination, Ph.D. dissertation, WHOI-88-10, 365 pp., Jan. 1988.

Wacongne, S., Dynamical regimes of a fully nonlinear stratified model of the Atlantic equatorial undercurrent, *J. Geophys. Res.*, *94*, 4801–4815, 1989.

Weingartner, T. J., and R. H. Weisberg, On the equatorial cycle of equatorial upwelling in the central Atlantic Ocean, *J. Phys. Oceanogr.*, *21*, 68–82, 1991.

Weisberg, R. H., and T. J. Weingartner, On the baroclinic response of the zonal pressure gradient in the equatorial Atlantic Ocean, *J. Geophys. Res.*, *91*, 11,717–11,725, 1986.

Weisberg, R. H., and T. J. Weingartner, Instability waves in the equatorial Atlantic Ocean, *J. Phys. Oceanogr.*, *18*, 1641–1657, 1988.

Weisberg, R. H., J. H. Hickman, T. Y. Tang, and T. J. Weingartner, Velocity and temperature observations during the seasonal response of the equatorial Atlantic Experiment at 0°, 28°W, *J. Geophys. Res.*, *92*, 5061–5075, 1987.

Wilson, D. and A. Leetmaa, Acoustic Doppler current profiling in the equatorial Pacific, *J. Geophys. Res.*, *93*, 13,947–13,966, 1988.

Wunsch, C., An estimate of the upwelling rate in the equatorial Atlantic based on the distribution of bomb radiocarbon and quasi-geostrophic dynamics, *J. Geophys. Res.*, *89*, 7977–7988, 1984.

Yoo, J. M., and J. A. Carton, Annual and interannual variation of the freshwater budget in the tropical Atlantic Ocean and the Caribbean Sea, *J. Phys. Oceanogr.*, *20*, 831–845, 1990.

Y. Gouriou, Woods Hole Oceanographic Institution, Woods Hole, MA 02543.

G. Reverdin, Lamont-Doherty Geological Observatory, Palisades, NY 10964.

(Received April 9, 1991;
revised August 12, 1991;
accepted October 16, 1991.)